KU LEUVEN

FACULTY OF ENGINEERING

Nonlinear Dynamics Report

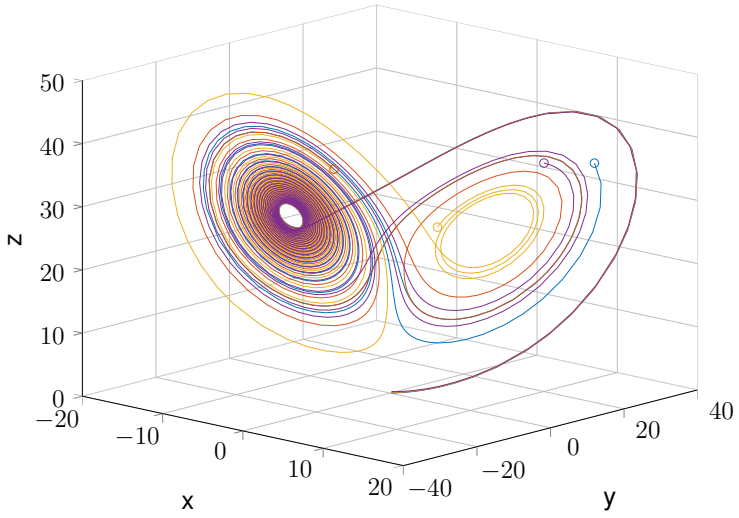

Moritz Wolter

Contents

Chapter 1

Laser Model

1.1 The equations

$$\dot{n} = GnN - kn. \tag{1.1}$$
$$\dot{N} = -GnN - fN + p. \tag{1.2}$$

1.2 First Order Analysis

Assume that the number of excited atoms remains quasi-static.

$$\dot{N} \approx 0. \tag{1.3}$$
$$\Rightarrow \dot{n} = Gn \cdot \frac{p}{Gn + f} - kn. \tag{1.4}$$
$$\tag{1.5}$$

1.2.1 Linear Stability analysis

In the two dimensional case fixed points are at the intersections of the first derivative with the real axis. Thus they can be found by solving $\dot{n} = 0$. Leading to the problem:

$$0 = n(\frac{Gp}{Gn + f} - k) \tag{1.6}$$

Which has the zeros 0 and $\frac{p}{k} - \frac{f}{G}$. To learn more about the nature of the fixed points one has to set the derivative of 1.4 to zero. Using the Quotient rule the expression;

$$\ddot{n} = \frac{Gfp}{(Gn + f)^2} - k \tag{1.7}$$

is obtained. A fixed point is stable if the second derivative is negative. Likewise it is unstable if the second derivative is positive [1]. Evaluating the second derivative for the fixed point a zero leads to $\ddot{n}(0) = \frac{Gp}{f} - k$ which leads to a values of $p_c = \frac{fk}{G}$. Thus the fixed points becomes unstable if $p > p_c$.

Figure 1.1 indicates a trans-critical bifurcation.

[1] Strogatz, p.25

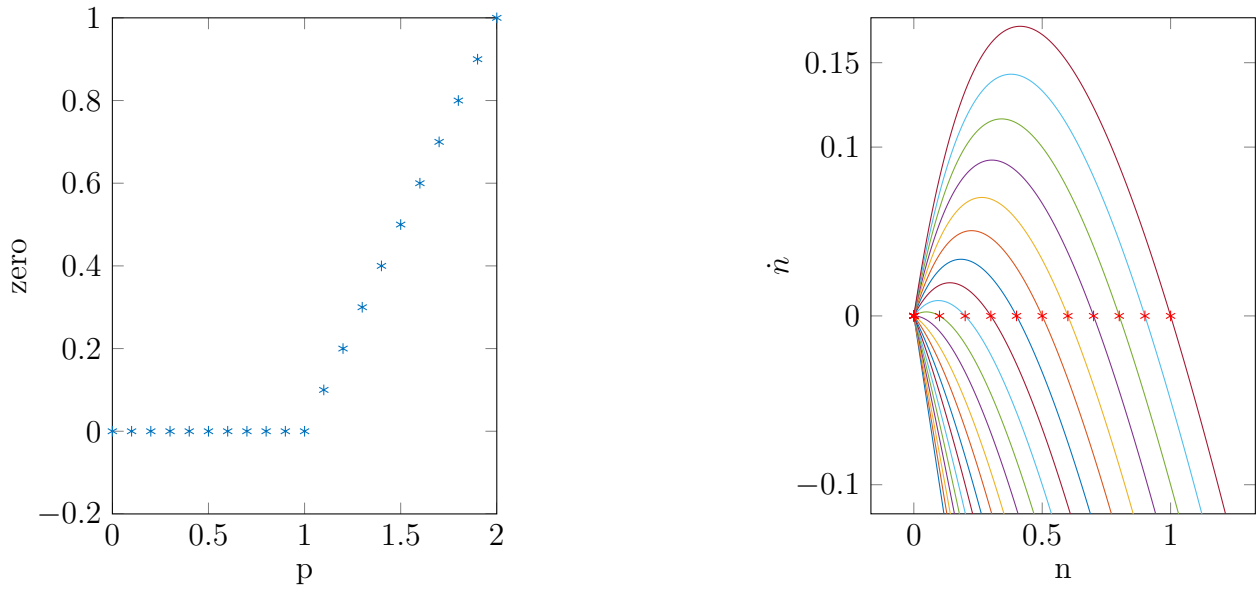

Figure 1.1: Plot of the position of the right zero and the parameter p (left). Plot of $\dot{n}$ for different p values with the zeros marked with red stars. $G = f = k = 1$ is assumed, leading to $p_c = 1$.

1.3 Two dimensional analysis

1.3.1 Nondimensionalization

To reduce the amount of parameters and simplify the analysis the system is non-dimensionalized. In a first step scaling parameters are introduced:

$$\tau = \frac{t}{\gamma} \quad x = \frac{n}{\alpha} \quad y = \frac{N}{\beta}. \tag{1.8}$$

$$\Rightarrow t = n\tau \quad n = x\alpha \quad N = y\beta \tag{1.9}$$

Using the chain rule for the derivatives leads to $\dot{n} = \frac{dn}{dt} = \frac{dn}{d\tau} \cdot \frac{d\tau}{dn} = \frac{dn}{d\tau} \cdot \frac{1}{\gamma} = \frac{dx}{d\tau} \cdot \frac{\alpha}{\gamma} = \hat{x}\frac{\alpha}{\gamma}$. Following a similar derivation for $\hat{y}$ and substituting leads to:

$$\hat{x} = Gxy\beta\gamma - kx\gamma \tag{1.10}$$

$$\hat{y} = -Gx\alpha y\gamma - fy\gamma + \frac{p\gamma}{\beta}. \tag{1.11}$$

Now the equations may be simplified by setting groups of coefficients to one. This choice determines the position of the constants. Several options exist:

1.3.2 The naïve approach

Ensuring the non-dimensionality of the system the last group in equation 1.11 is set to one. Next the last group in 1.10 is set to one. Now the remaining options are only the first terms of the two equations. Somewhat arbitrarily the first group of the second equation

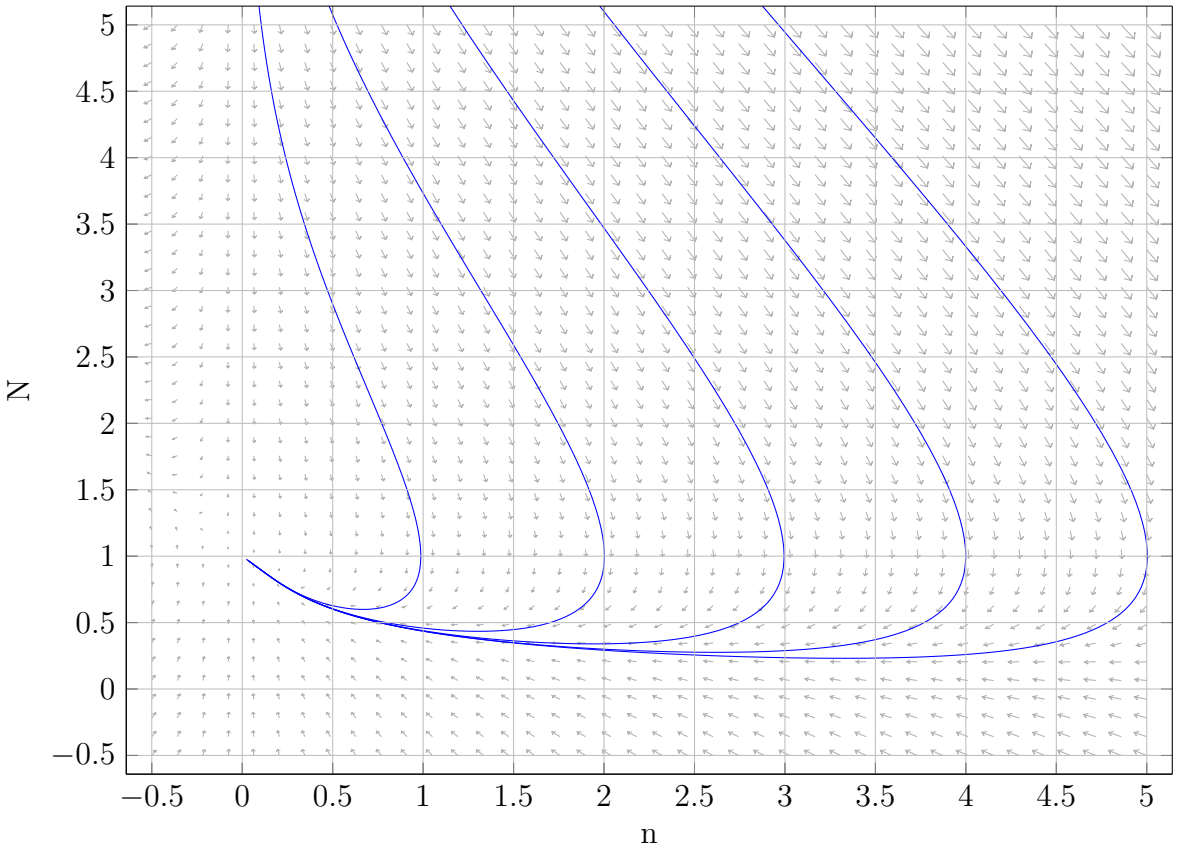

Figure 1.2: Phase plane of the original system $n' = GnN - kn \quad N' = -GnN - fN + p$, which an uncritical choice for the parameters $p < p_c$. $(f = k = G = p = 1)$

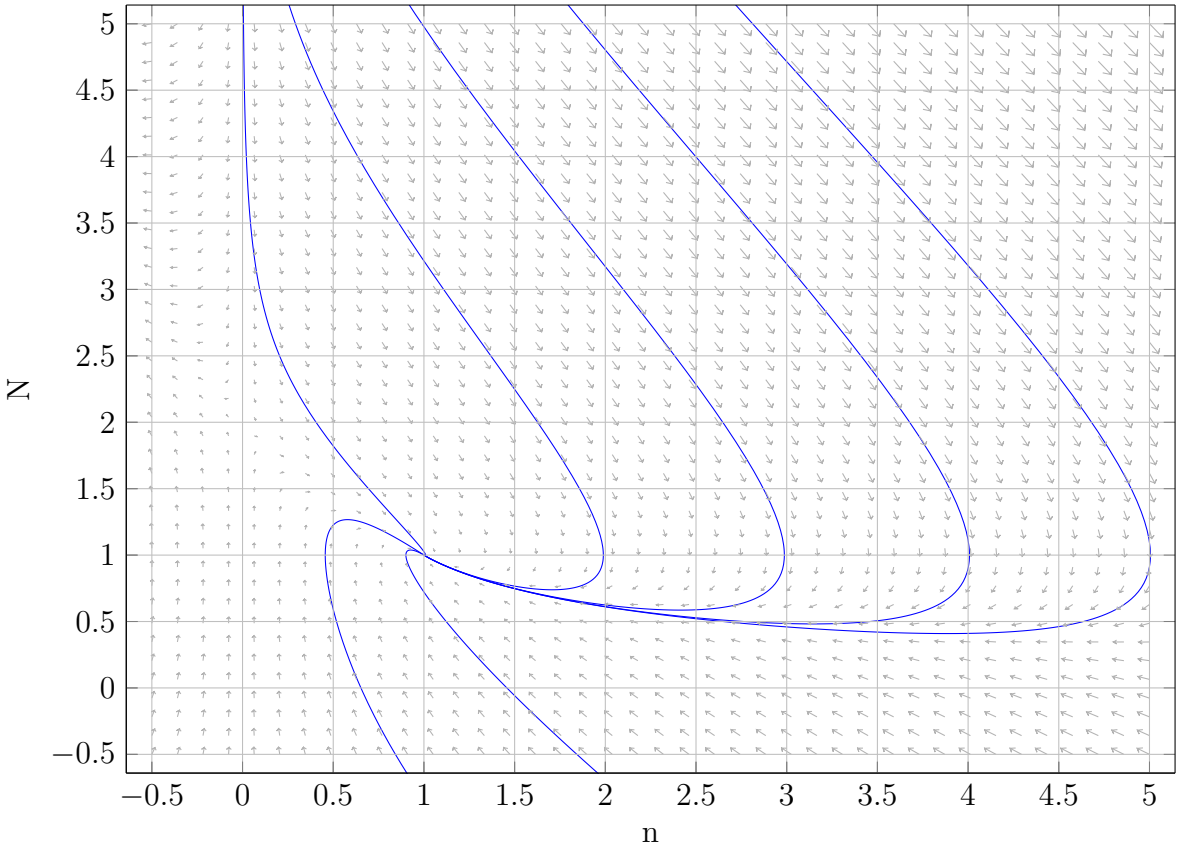

Figure 1.3: Phase plane of the original system $n' = GnN - kn \quad N' = -GnN - fN + p$, with $p < p_c$.$(f = k = G = 1 \;\; p = 2)$

$\mathbf{x}_1^* = \begin{pmatrix} 0 \\ \frac{1}{c_2} \end{pmatrix}$	$\tau_1 = \frac{c_1}{c_2} - c_2 - 1$	$\triangle_1 = c_2 - c_1$
$\mathbf{x}_2^* = \begin{pmatrix} -c_2 + c_1 \\ \frac{1}{c_1} \end{pmatrix}$	$\tau_2 = -c_1$	$\triangle_2 = c_1 - c_2$

Table 1.1: Fixed points, Jacobi trance and determinant as found by using the naïve approach.

is set to one. This leads to:

$$\frac{p\gamma}{\beta} = 1 \tag{1.12}$$

$$k\gamma = 1 \tag{1.13}$$

$$G\alpha\gamma = 1. \tag{1.14}$$

Solving for the scaling parameters and substituting the remaining system parameters with c_1 and c_2 leads to:

$$\hat{x} = c_1 xy - x. \tag{1.15}$$

$$\hat{y} = -xy - c_2 y + 1. \tag{1.16}$$

Now the fixed points can be determined by solving for the zero vector $\begin{pmatrix} 0 & 0 \end{pmatrix}^T$:

$$\mathbf{x}_1^* = \begin{pmatrix} 0 \\ \frac{1}{c_2} \end{pmatrix} \tag{1.17}$$

$$\mathbf{x}_2^* = \begin{pmatrix} -c_2 + c_1 \\ \frac{1}{c_1} \end{pmatrix}. \tag{1.18}$$

Above $c_1 = \frac{Gp}{k^2}$ and $c_2 = \frac{f}{k}$. To learn more about the nature of these points the Jacobi-matrix is computed, which is done by computing the partial derivative with respect to x in the first and to y in the second column.

$$J = \begin{pmatrix} yc_1 - 1 & xc_1 \\ -y & -x - c_2. \end{pmatrix} \tag{1.19}$$

This matrix my now be evaluated at the fixed points, so $J(\mathbf{x}_1^*)$ and $J(\mathbf{x}_2^*)$ are computed. From here the nature of the fixed points can be classified by looking at the trace τ and the determinant $\triangle$. The results are tabulated in table 1.1.

1.3.3 The smart approach

In an attempt to simplify the expressions obtained the scaling parameters will be gouped differently. From the Jacobi matrix given in equation 1.19 it follows that the factors before the xy terms show up twice in the matrix. Coefficients that scale a single x or y terms appear once, while the constant disappears fully. However to keep the equations dimensionless the constant term has to remain one. Thus the remaining two groups before

$x_1^* = \begin{pmatrix} 0 \\ \frac{1}{c_2} \end{pmatrix}$	$\tau_1 = \frac{1}{c_2} - c_1 - c_2$	$\triangle_1 = c_1 c_2 - 1$
$x_2^* = \begin{pmatrix} \frac{1-c_1 c_2}{c_1} \\ c_1 \end{pmatrix}$	$\tau_2 = -\frac{1}{c_1}$	$\triangle_2 = -c_1 c_2 + 1$

Table 1.2: Results obtained by using the smart method.

the high-frequent xy terms will be set to one. Starting from equations 1.10 and 1.11, a similar process as the one outlined above is followed, which leads to the system:

$$\hat{x} = xy - c_1 x \tag{1.20}$$

$$\hat{y} = -xy - c_2 y + 1 \tag{1.21}$$

With the two constants $c_1 = \sqrt{\frac{k^2}{Gp}}$ and $c_2 = \sqrt{\frac{f^2}{Gp}}$. And the fixed points turn out to be $x_1^* = \begin{pmatrix} 0 & \frac{1}{c_2} \end{pmatrix}^T$ and $x_2^* = \begin{pmatrix} \frac{1-c_1 c_2}{c_1} & c_1 \end{pmatrix}^T$. This new system leads indeed to a simpler Jacobi matrix, which is given by:

$$J = \begin{pmatrix} y - c_1 & x \\ -y & -x - c_2 \end{pmatrix} \tag{1.22}$$

Again the Jacobi matrix is evaluated at the fixed points, results are given in table 1.2. Unfortunately, the obtained expressions are not simpler then those computed earlier. Additionally the new c_1 and c_2 will turn imaginary for negative p. However this approach does add another angle to the interpretation of the results.

1.3.4 Interpretation

Fixed point position

Due to the rescaling of the axes that has been performed naturally the position of the fixed points changes, however their properties will remain unchanged. Instead of the original position at

$$\mathbf{n}_1^* = \begin{pmatrix} 0 \\ \frac{p}{f} \end{pmatrix} \tag{1.23}$$

$$\mathbf{n}_2^* = \begin{pmatrix} -\frac{f}{G} + \frac{p}{k} \\ \frac{k}{G} \end{pmatrix} \tag{1.24}$$

The fixed points will appear at:

$$\mathbf{x}_1^* = \begin{pmatrix} 0 \\ \frac{p}{f\beta} \end{pmatrix} \tag{1.25}$$

$$\mathbf{x}_2^* = \begin{pmatrix} -\frac{f}{G\alpha} + \frac{p}{k} \\ \frac{k}{G\beta} \end{pmatrix} \tag{1.26}$$

after the rescaling process. The new position depends on the scaling parameters α and β.

condition	trace	determinant	fixed point classification	spiral
$p = p_c$	$\tau_1 < 0$	$\triangle_1 = 0$	$\mathbf{x}_1^*$ non-isolated stable fixed point	no
$c_1 = c_2$	$\tau_2 < 0$	$\triangle_2 = 0$	$\mathbf{x}_2^*$ non-isolated stable fixed point	no
$p > p_c$	$\tau_1 > -c_2$	$\triangle_1 < 0$	$\mathbf{x}_1^*$ saddle point	
$c_1 > c_2$	$\tau_2 < 0$	$\triangle_2 > 0$	$\mathbf{x}_2^*$ stable fixed point	if $\tau^2 - 4\triangle < 0$
$p < p_c$	$\tau_1 < -c_2$	$\triangle_1 > 0$	$\mathbf{x}_1^*$ stable fixed point	if $\tau^2 - 4\triangle < 0$
$c_1 < c_2$	$\tau_2 < 0$	$\triangle_2 < 0$	$\mathbf{x}_2^*$ saddle point	

Table 1.3: Classification of fixed points using the results from the naïve approach

Bifurcations

Since the results from the smart approach do not turn out to be simpler then those found with the first one. The formulations from table 1.1 will be used during the subsequent analysis. Starting from the condition for p_c:

$$p = p_c \tag{1.27}$$
$$p = \frac{fk}{G} \tag{1.28}$$
$$Gp = fk \tag{1.29}$$
$$\frac{Gp}{k} = f \tag{1.30}$$
$$\frac{Gp}{k^2} = \frac{f}{k} \tag{1.31}$$
$$\Leftrightarrow c_1 = c_2. \tag{1.32}$$

Using the same procedure for $p > p_c$ yields $c_1 > c_2$ and $p < p_c$ leads to $c_1 < c_2$. Armed with these new inequalities it is now possible to proceed with the evaluation of the expressions given in table 1.1. Results are shown in 1.3. A plot of the conditions from table 1.3 is given in 1.5.

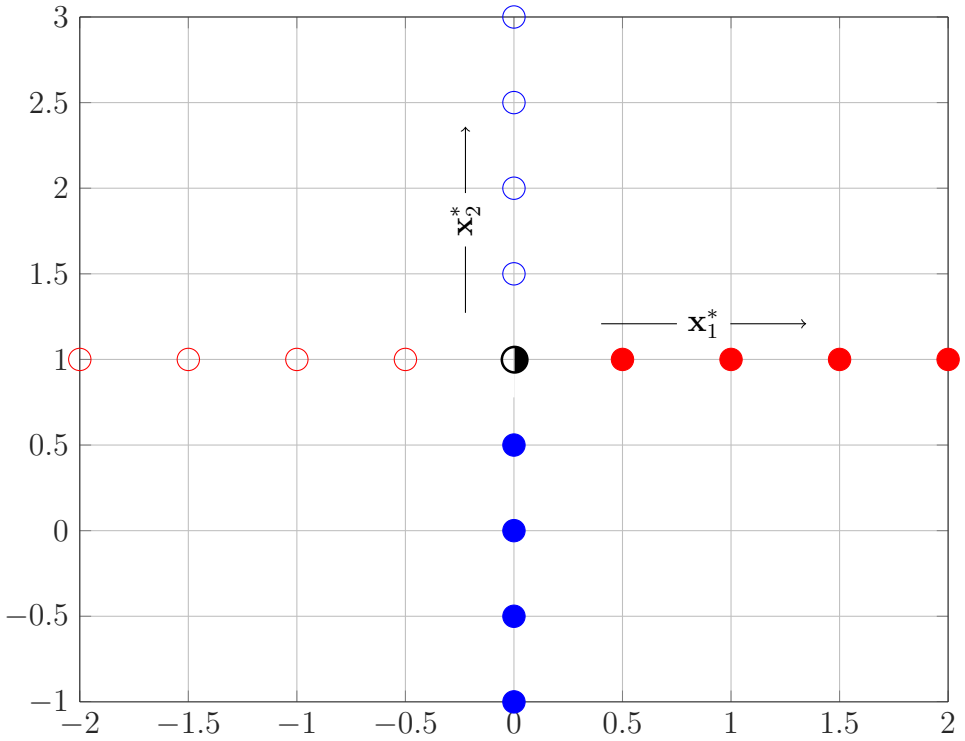

Figure 1.4: Bifurcation diagram for the given system with $f = k = G = 1$ and $p \in (-1, 3)$. The filled circles indicate stable attracting fixed points. The empty ones symbolize a saddle point. The half filled circle represents a bifurcation.

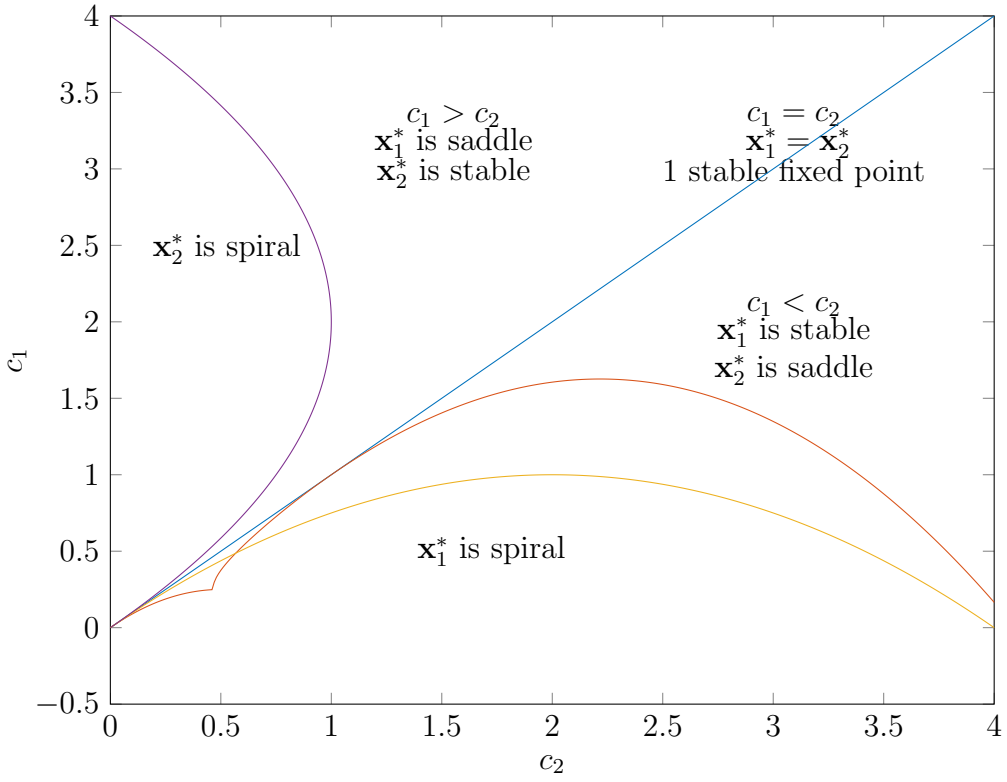

Figure 1.5: Stability diagram showing the results from table 1.3

Chapter 2

Bridge Oscillations

In this chapter the effects of wind on a poorly designed bridge will be explored.

2.1 Equation of Motion

The model for the structure leads to the following equation of motion:

$$0 = -F_I - F_d - F_e + F_{dr} \tag{2.1}$$

$$0 = -m\ddot{y} - r\dot{y} - ky + \frac{1}{2}\rho V^2 a C(\alpha). \tag{2.2}$$

Where $C(\alpha)$ is a nonlinear function.

2.2 Linear Analysis

$C(\alpha)$ is defined as a sum of several odd powers of α:

$$C(\alpha) = A_1\alpha - \underbrace{A_3\alpha^3 + A_5\alpha^5 - A_7\alpha^7.}_{\approx 0 \text{ for small } \alpha.} \tag{2.3}$$

for small α additionally the approximation $\alpha = \frac{\dot{y}}{V}$ is given. Plugging into 2.2 yields:

$$0 = -m\ddot{y} + (\frac{1}{2}\rho V a A_1 - r)\dot{y} - ky. \tag{2.4}$$

Which may be rewritten in terms of two first order equations:

$$\begin{pmatrix}\dot{x}\\ \dot{y}\end{pmatrix} = \begin{pmatrix}\frac{\frac{1}{2}\rho V a A_1 - r}{m} & -\frac{k}{m}\\ 1 & 0\end{pmatrix}\begin{pmatrix}x\\ y\end{pmatrix} \tag{2.5}$$

Setting the derivatives to zero the fixed point $\mathbf{x}_1^* = \begin{pmatrix}0 & 0\end{pmatrix}^T$ is obtained. As a linear approximation has already taken place the Jacobi-matrix is identical to the system matrix given above. Thus for the trace τ_1 and determinant $\triangle_1$ at the fixed point the following equations are obtained:

$$\tau_1 = \frac{\frac{1}{2}\rho V a A_1 - r}{m} - \frac{k}{m} \tag{2.6}$$

$$\triangle_1 = \frac{k}{m}. \tag{2.7}$$

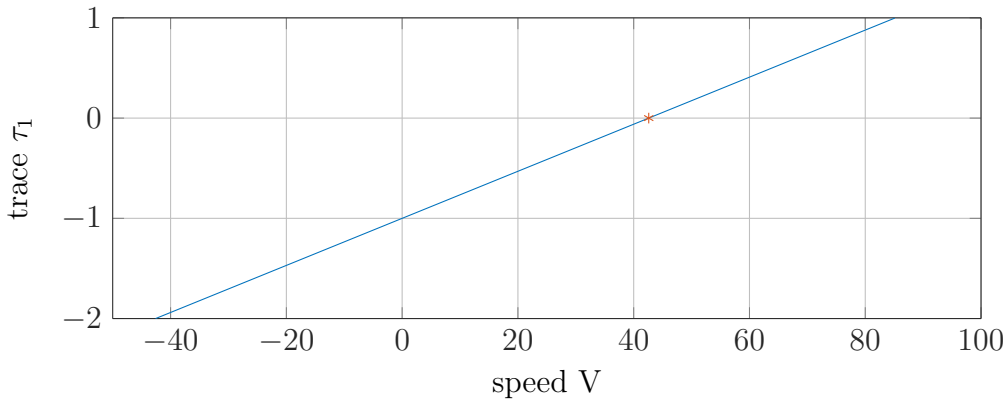

Figure 2.1: Plot of τ_1 for different speed values. The critical wind speed V_c is marked with a red asterisk.

Assuming $(k \wedge m) > 0$ the nature of the fixed point is determined by the trace. The critical value will occur for $\tau_1 = 0$, therefore it may be found from:

$$0 = \frac{1}{2}\frac{\rho V^2 a A_1}{m V_c} - \frac{r}{m}. \tag{2.8}$$

Solving for V_c leads to:

$$V_c = \frac{2r}{\rho a A_1} = 42.5985. \tag{2.9}$$

When $m = 1,\ \rho = 1,\ r = 1\ k = 100,\ a = 1$ and $A_1 = 100$. A plot for τ_1 with respect for different values for V is given in figure 2.1. As the determinant remains positive at all times the fixed point at the center changes from a stable to an unstable spiral at the critical wind speed V_c.

2.3 Simulation of the non-linear System

In this section simulation will be attempted without linearization. Including all terms the following system of first order ordinary differential equations is obtained:

$$\dot{y} = z \tag{2.10}$$

$$\dot{z} = -\frac{ky}{m} - \frac{rz}{m} + \frac{1}{2}\frac{\rho V^2 a}{m}[A_1\frac{z^1}{V^1} - A_3\frac{z^3}{V^3} + A_5\frac{z^5}{V^5} - A_7\frac{z^7}{V^7}]. \tag{2.11}$$

Equation 2.11 may be simulated in matlab using an explicit Runge-Kutta type solver (`ode45`). Results are given in figures 2.5,2.6 and 2.7.

2.4 Comparison of linear and nonlinear dynamics around V_c

Setting $m = \rho = r = a = 1$ yields the simplified version of equation 2.4 for the linear case at critical speed V_c:

$$0 = -\ddot{y} + (\frac{1}{2}V_c A_1 - 1)\dot{y} - ky. \tag{2.12}$$

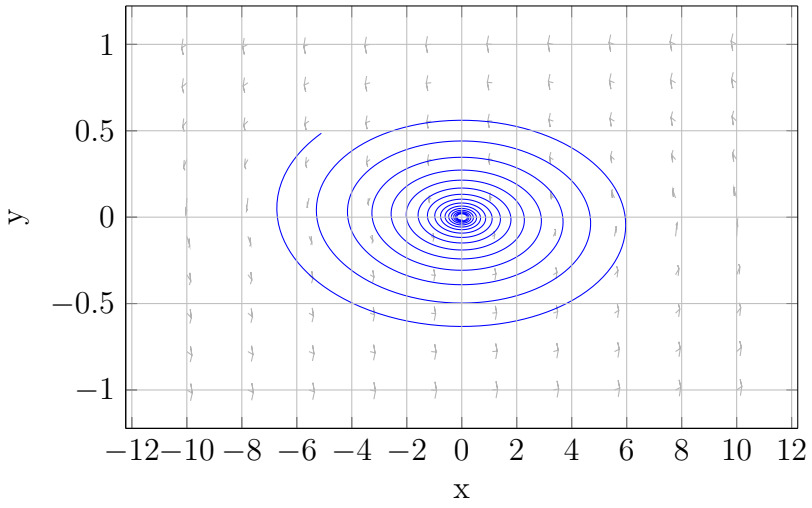

Figure 2.2: Plot of the two dimensional linearized system with $V = 10 < V_c$.

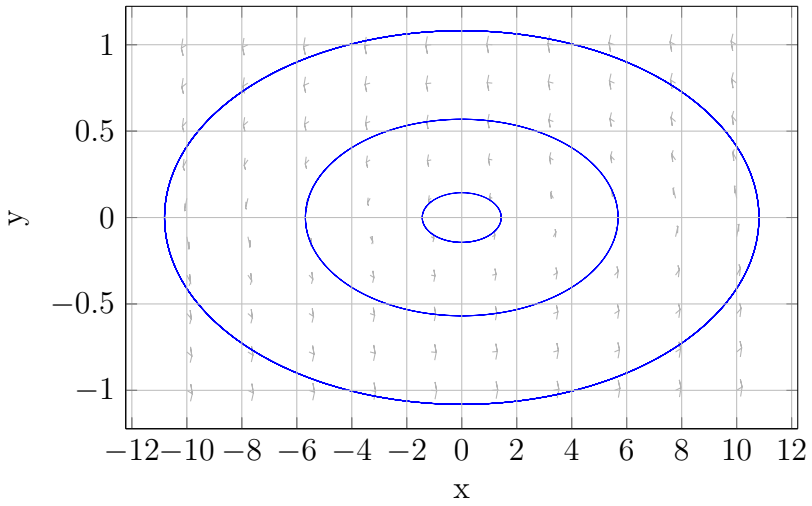

Figure 2.3: Plot of the two dimensional linearized system with $V = 42.5985 = V_c$.

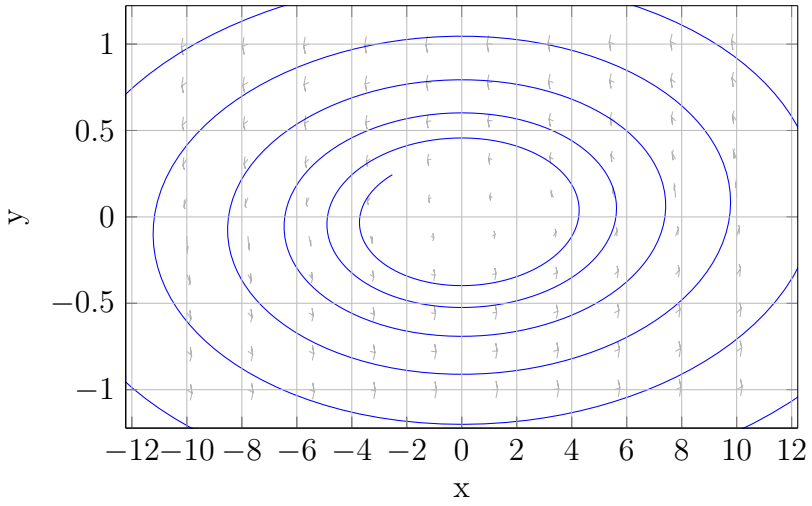

Figure 2.4: Plot of the two dimensional linearized system with $V = 80 > V_c$.

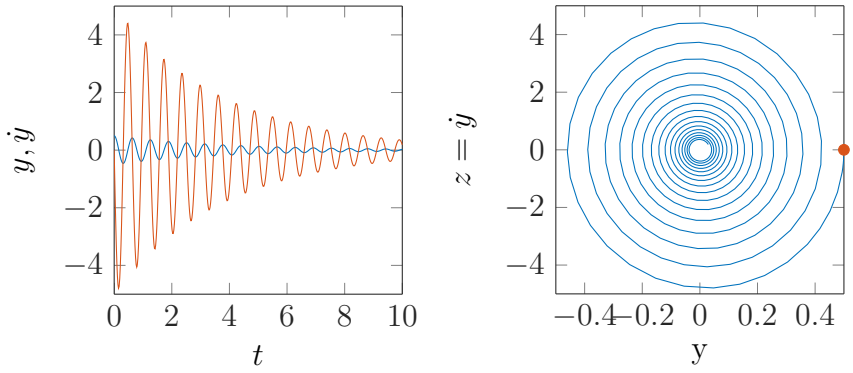

Figure 2.5: Nonlinear simulation results shown as time plot (left) and in their phase plane representation (right) for $V = 20 < V_c$. In the left plot bridge position is shown in blue. The first derivative is depicted in red. In the right plot the initial condition is depicted as a red dot.

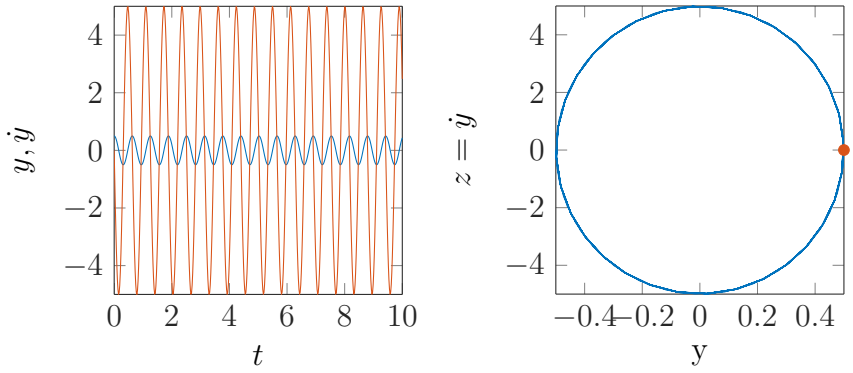

Figure 2.6: Nonlinear simulation results shown as time plot and in their phase plane representation for $V = V_c$.

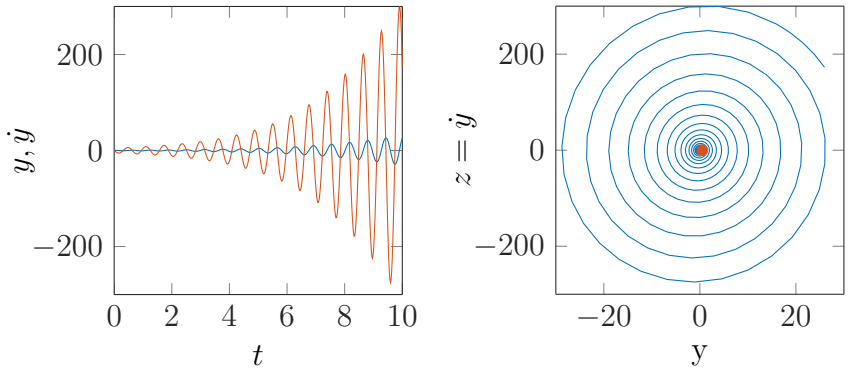

Figure 2.7: Nonlinear simulation results shown as time plot and in their phase plane representation for $V = 80 > V_c$.

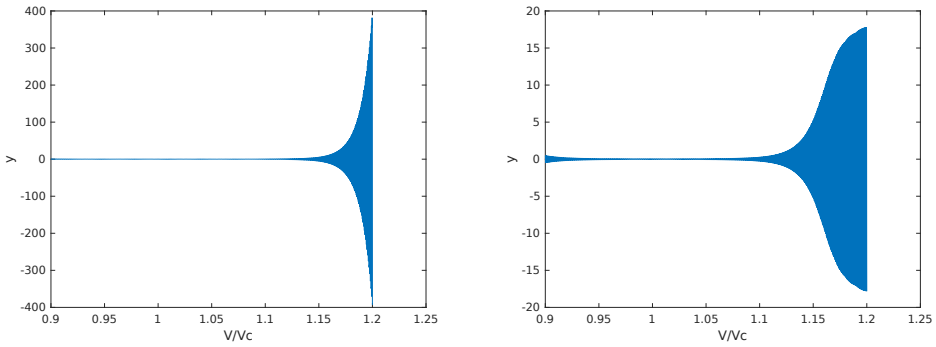

Figure 2.8: Linear(left) and nonlinear(right) model simulation results for wind speed values close to V_c

Given that V_c simplifies to $V_c = \frac{2}{A_1}$ the linear approximation predicts the term for the first derivative to be zero. However in the nonlinear case one obtains:

$$0 = -\ddot{y} + \underbrace{(\frac{1}{2}V_c A_1 - 1)}_{=0}\dot{y} - ky + \underbrace{\frac{1}{2}V_c^2(-A_3\frac{z^3}{V_c^3} + A_5\frac{z^5}{V_c^5} - A_7\frac{z^7}{V_c^7})}_{\neq 0} \tag{2.13}$$

The additional nonlinear terms will move the position of the bifurcation points slightly. Furthermore this polynomial will exhibit quite different growth behavior in comparison to it's linear counter part. An expectation, which can indeed be confirmed by simulation. Figure 2.8 shows the linear and nonlinear model dynamics for wind speed values close to V_c.

2.5 Limit cycle and bifurcation analysis

So far only a bifurcation with respect to the stability of the fixed point at the origin has been discovered. However a closer look at the system's eigenvalues will reveal another interesting property. Considering the expression derived in 2.5 the eigenvalues are:

$$\lambda_{1,2} = -\frac{1}{2} + \frac{1}{4}VA_1 \pm \sqrt{(\frac{1}{2} - \frac{1}{4}VA_1)^2 - 1} \tag{2.14}$$

The interesting part is the one underneath the square root. If this part turns negative the eigenvalues of the Jacobian become complex, which would lead to a Hopf-bifurcation

[1]. Thus the following condition is derived:

$$(\frac{1}{2} - \frac{1}{4}VA_1)^2 - 1 < 0 \tag{2.15}$$

$$(\frac{1}{2} - \frac{1}{4}VA_1)^2 < 1 \tag{2.16}$$

$$(\frac{1}{2} - \frac{1}{4}VA_1) < 1 \tag{2.17}$$

$$\frac{1}{2} < \frac{1}{4}VA_1 \tag{2.18}$$

$$\frac{2}{A_1} < V \tag{2.19}$$

$$\tag{2.20}$$

This new inequality is true when V surpasses V_c. Using equation 2.9:

$$V_c < V. \tag{2.21}$$

Thus the first bifurcation is a Hopf-bifurcation. Figures 2.9, 2.10, 2.11 and 2.12 explore what happens after this first Hopf bifurcation.

[1]book page 251

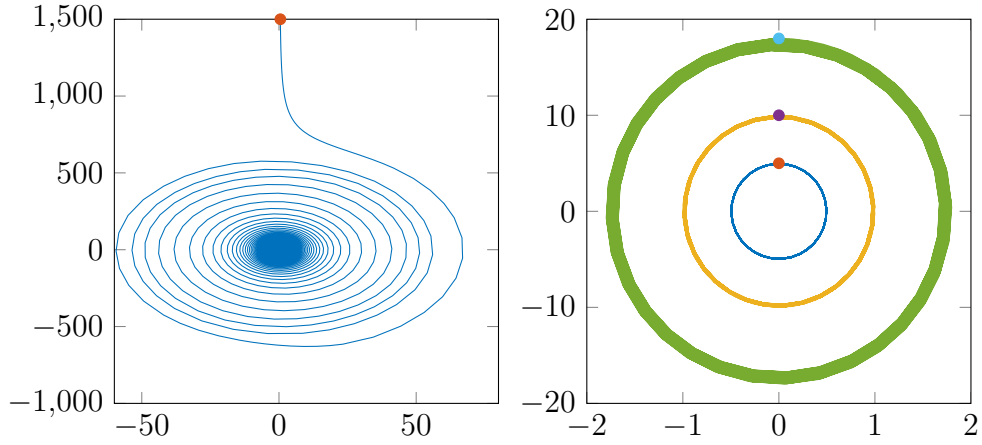

Figure 2.9: Initial situation with $V = 0.9 < V_c$ (left). The fixed point at the origin is stable.$V = 1 = V_c$ (right). Initial conditions within the green circle oscillate forever.

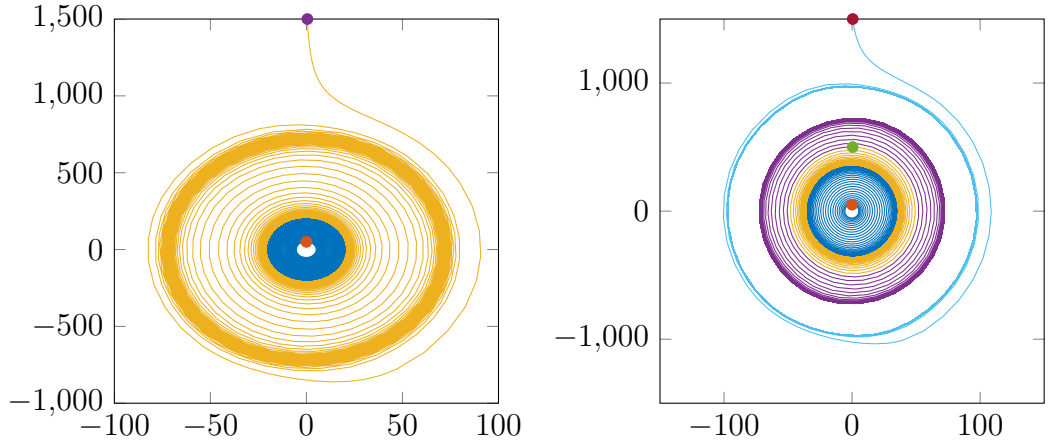

Figure 2.10: $V = 1.2 > V_c$ the Hopf bifurcation has occurred and a yellow ghost foreshadows another event (left). $V = 1.5 > V_c$ the ghost reveals a cyclic saddle node bifurcation, as the backward solution of the initial condition at $(0, 500)$ shown in purple hits another boundary (right).

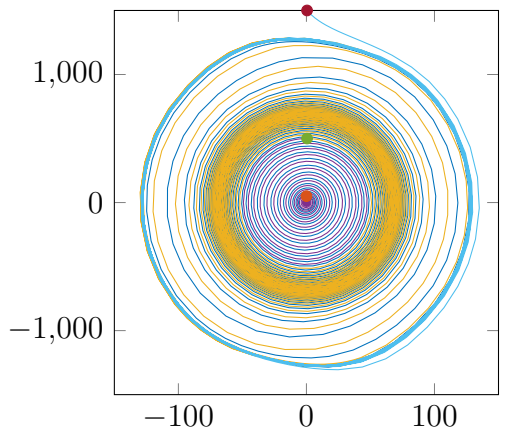

Figure 2.11: $V = 1.9 > V_c$ the two inner circles have collided and annihilated each other leaving behind another ghost that slows trajectories in its vicinity.

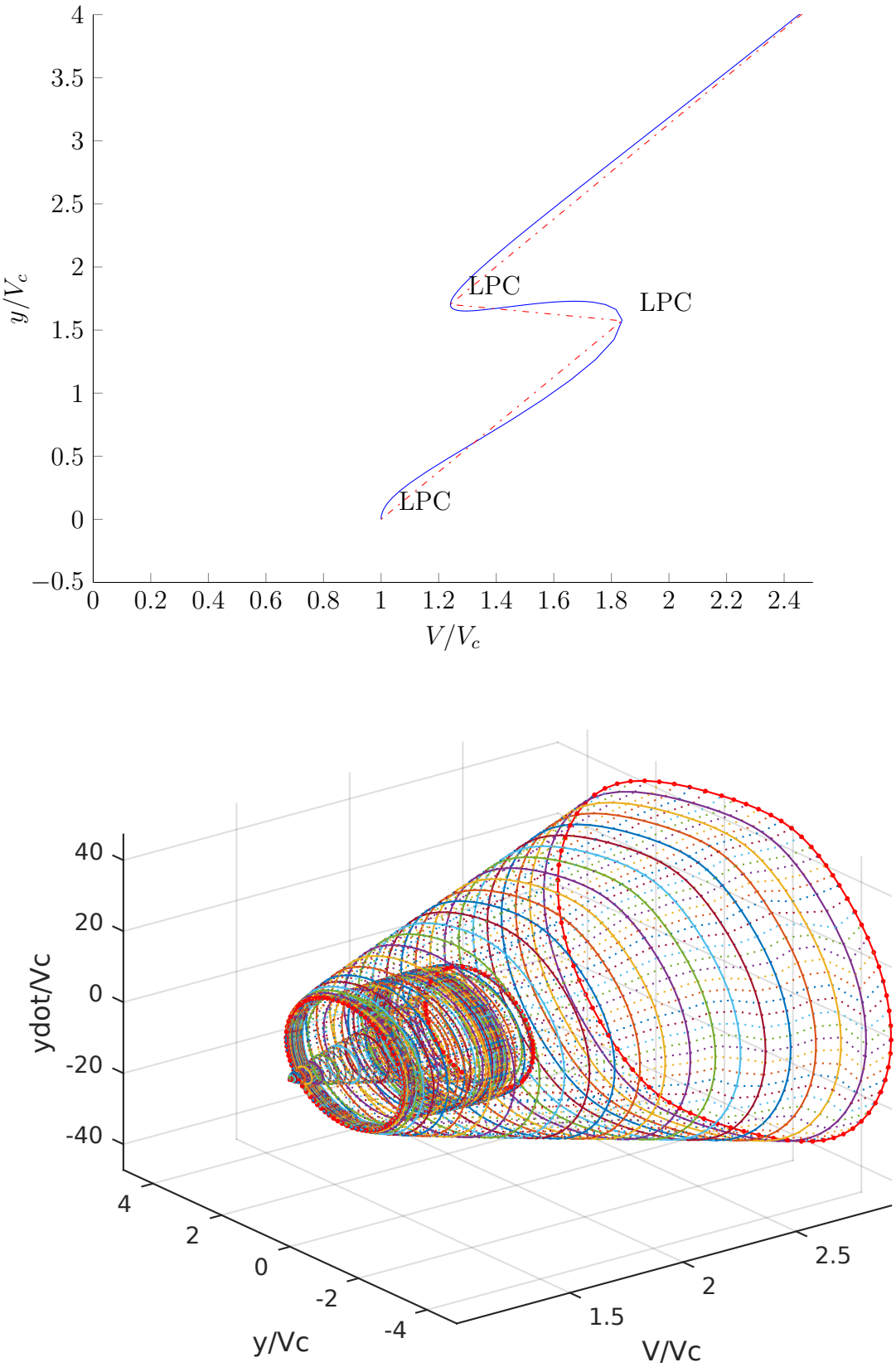

Figure 2.12: `matcont` output. The top plot an excerpt of the bottom 3D-graphic. The two additional bifurcation points 1.243 and 1.823 can be read off.

Chapter 3

Imperfect bifurcations

3.1 The equation

$$-\frac{1}{2}u^3 + ru + h = 0. \tag{3.1}$$

3.2 Bifurcation analysis

3.2.1 Manual analysis

Bifurcation analysis means looking at fixed point movement and the evolution of their stability. In this report equation 3.1 will be analyzed thoroughly. It contains the information of the fixed point locations for the system:

$$\dot{u} = -\frac{1}{2}u^3 + ru + h. \tag{3.2}$$

`matcont` may be used to do this kind of analysis. However to put the results into perspective. A manual analysis has been performed beforehand [1]. Figures 3.1,3.2 3.3 show each a graphical approach to find the zeros of 3.1 in the first column. The second column shows the evolution of the position of the zeros. For different values for the imperfection parameter $h = 5, 0$ and 1 as well as $r \in [-30, 30]$ with a step size of 0.1. Finally the last columns do the same for different values of h with r constant. Linear stability analysis may be employed to learn more about the system dynamics. The first derivative of $f(u) = -\frac{1}{2}u^3 + ru + h$ is:

$$f'(u) = -\frac{3}{2}u^2 + r. \tag{3.3}$$

At the extreme points the derivative is zero, which leads to $u_{max} = \sqrt{\frac{2}{3}r}$. Thus leading to the maximum values $f(u_{max}) = \frac{1}{3}\sqrt{\frac{2}{3}}r^{3/2}$. As bifurcations occur when h hits the local maximum values one obtains $h_c = \pm f(u_{max})$. In the second column of the figures 3.1,3.2 3.3 the effect of the imperfection parameter may be observed. $h = 0$ leads to a textbook pitchfork bifurcation. However if $h \neq 0$ the fork separates and a saddle node bifurcation occurs which one part moving up or down with respect to x depending on the parameter signs. Figure 3.4 is a three dimensional data representation. It contains all the

[1] see pages 70-73 in Strogatz' book

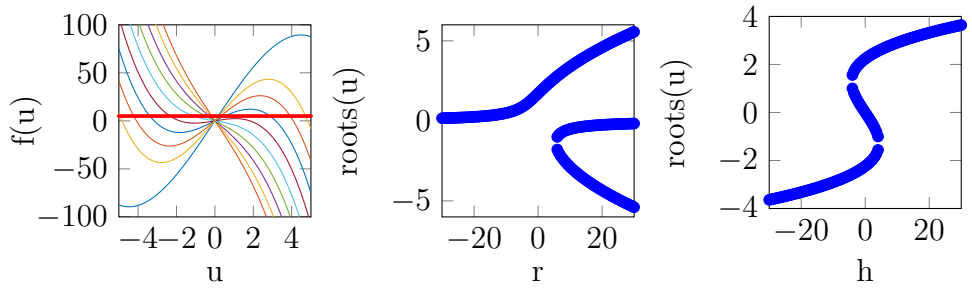

Figure 3.1: Solution branches with the function $-\frac{1}{2}u^3 + ru$ numerous colors for different $r \in [-30, 30]$ and the constant function $h = 5$ in red (left). Root locus plot for the same r values (center). Solution for different h with constant $r = 5$ (right).

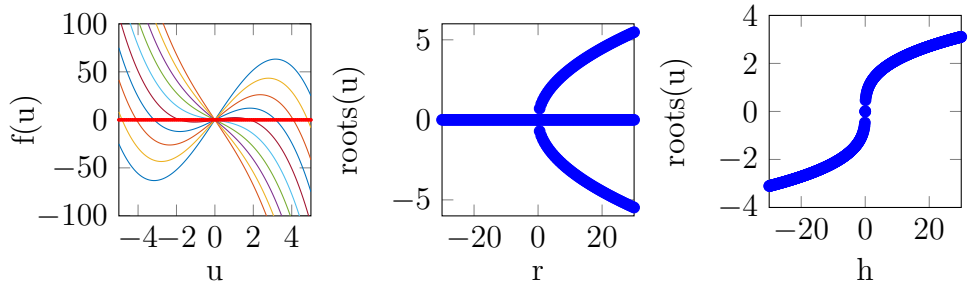

Figure 3.2: Solution branches with the function $-\frac{1}{2}u^3 + ru$ numerous colors for different $r \in [-30, 30]$ and the constant function $h = 0$ in red (left). Root locus plot for the same r values (center). Solution for different h with constant $r = 0$ (right).

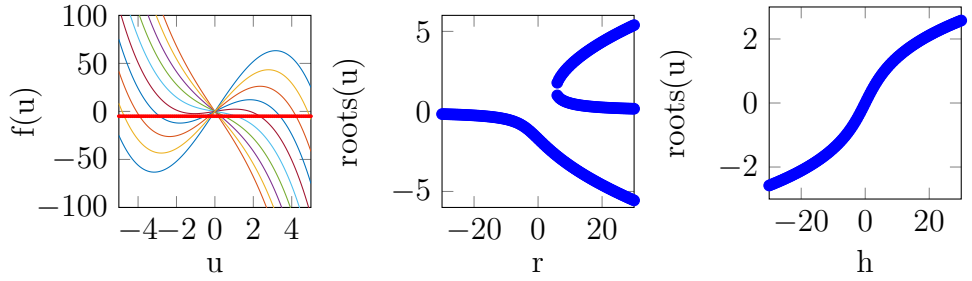

Figure 3.3: Solution branches with the function $-\frac{1}{2}u^3 + ru$ numerous colors for different $r \in [-30, 30]$ and the constant function $h = -5$ in red (left). Root locus plot for the same r values (center). Solution for different h with constant $r = -5$ (right).

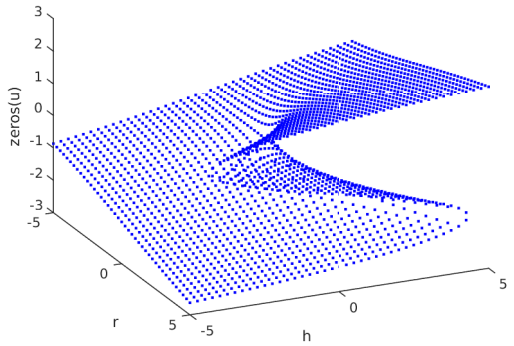

Figure 3.4: r, h, u plot of the polynomial roots.

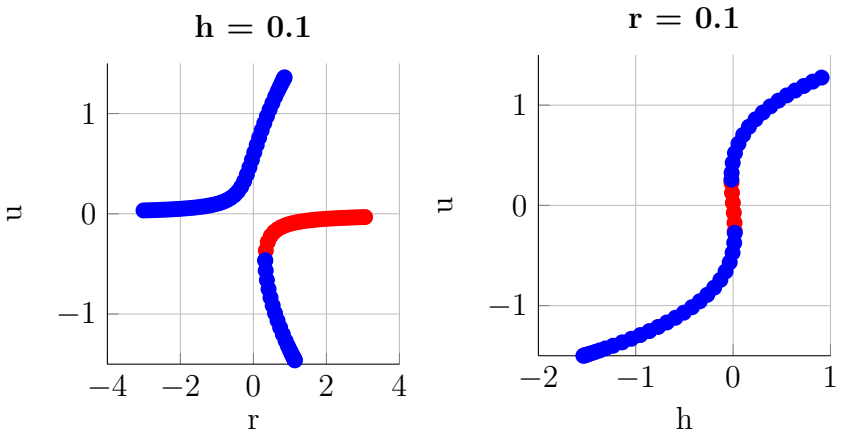

Figure 3.5: `matcont output for` $h = 0.1$

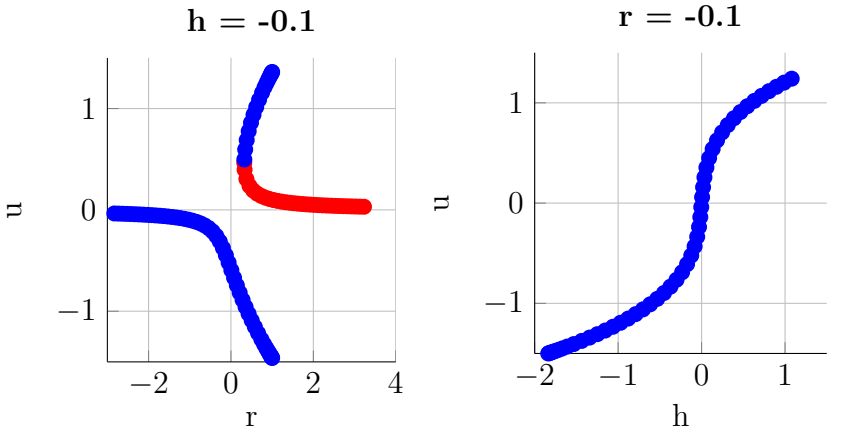

Figure 3.6: `matcont output for` $h = -0.1$

other plots either as cross sections or projections [2]. The saddle node bifurcation, which leads to the folded shape of the r, h plane.

3.2.2 `matcont` analysis

Figures 3.5 and 3.6, repeat the previous experiments using the `matcont` command line package. The computed figures are similarly shaped as those found previously. Thus it is assumed that computations are correct. The `matcont` package has the added benefit, that unstable points are distinguished from stable ones and drawn in red.

Figure 3.7 shows the position of the polynomials roots in the r, h-plane. The plot is called a stability diagram.

3.2.3 Step-size Experiment

Figure 3.8 shows computations results for two h values close to zero with the same `matcont parameters`. The second figure is presumably a correct computation as the results agree with those found in figure 3.3 and 3.6. The top plot is not correct. Instead of making the correct left turn the solution continues incorrectly onto the upper branch. This

[2] book strogatz page 73

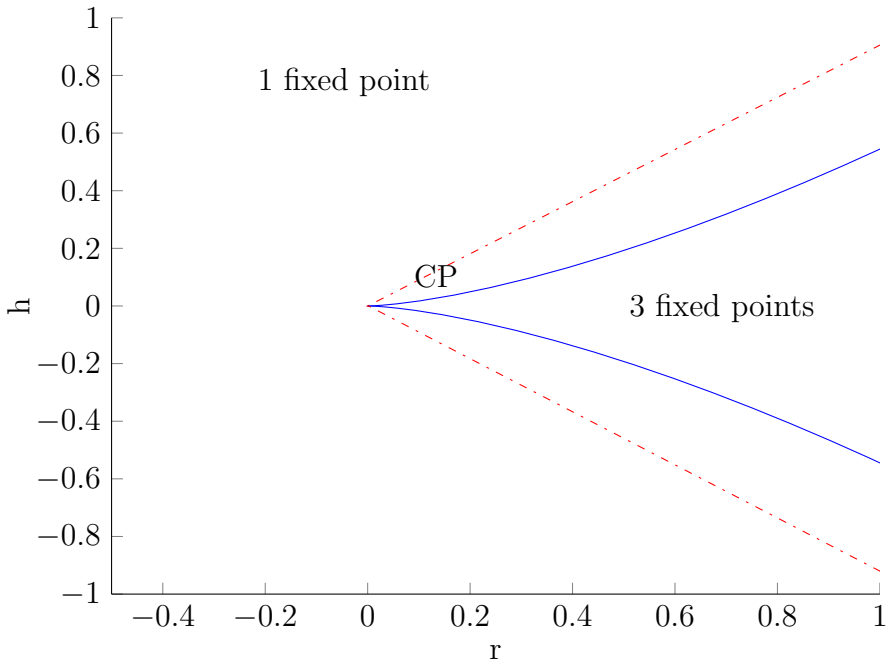

Figure 3.7: Evolution of the zeros within the r, h plane.

problem can be fixed by choosing a smaller step size and a higher point maximum. Incorrect solutions appear if input and stepsize differ too much in magnitude. Furthermore computations fails if the to little newton iterations are done if the upper limit for the computation points is set too low.

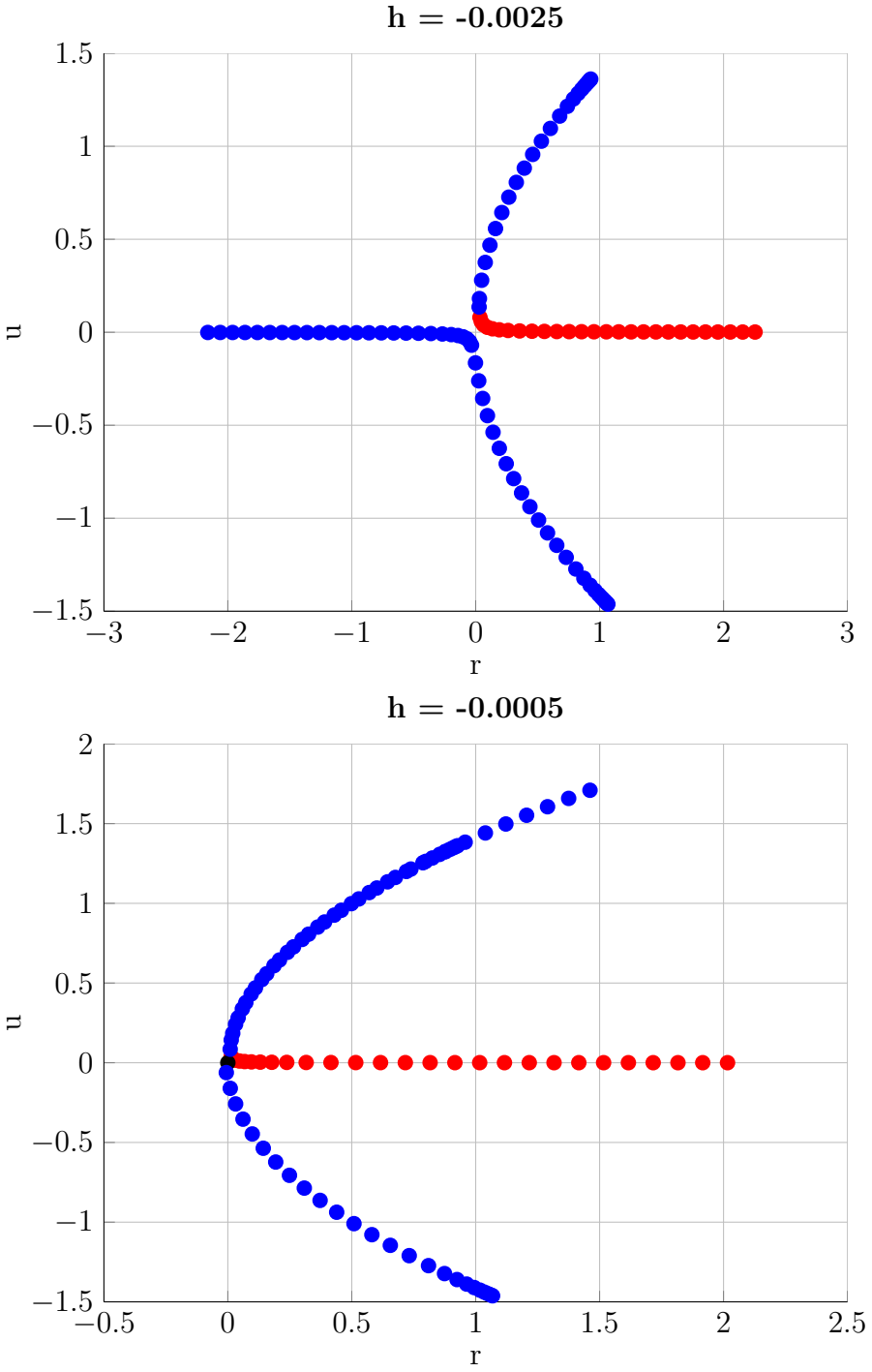

Figure 3.8: Solution branch of $h = -0.0025 \wedge -0.0005$. With `opt=contset(opt,'MinStepsize',0.01); opt=contset(opt,'MaxStepsize',0.1); opt=contset(opt,'MaxNewtonIters',4);`

Chapter 4

Study of a predator prey model

4.1 The equation

$$\dot{x} = x(x-a)(1-x) - bxy \tag{4.1}$$
$$\dot{y} = xy - cy - d. \tag{4.2}$$

With $a = 0.4,\ b = 0.3,$ and $c \in [0.650.75]$. x represents prey and y predators. The xy products of the system govern the interaction of the two species.

4.2 Analysis of a simplified model $d = 0$

4.2.1 One-dimensional approach

Setting d and y equal to zero turns the system into:

$$\dot{x} = x(x-a)(1-x). \tag{4.3}$$

For this simplified case the fixed points may be read off easily. $\dot{x} = 0$ yields $x_1 = 0,\ x_2 = a,\ x_3 = 1$. Linear analysis will lead to further insight into the nature of these fixed points reading of $f(x) = x(x-a)(1-x)$ and computing $f'(x)$ yields:

$$f'(x) = -3x^2 + 2x + 2xa - a. \tag{4.4}$$

Plugging in the fixed points for x:

$$f'(x_1) = -a \tag{4.5}$$
$$f'(x_2) = -a^2 + a = -0.4^2 + 0.4 > 0 \tag{4.6}$$
$$f'(x_3) = -3 + 2 + 2a - a = -1 + a = -0.6 < 0 \tag{4.7}$$

Thus it may be concluded, that x_2 is unstable and $x_3 \wedge x_1$ are stable. Figure 4.1 shows simulation results produced by a Runge-Kutta type numerical integration routine. The fixed point positions that where read off from the simplified system equation are confirmed by the results to be at $x_1 = 0,\ x_2 = a = 0.4,\ x_3 = 1$. Furthermore the fixed points show the predicted characteristics.

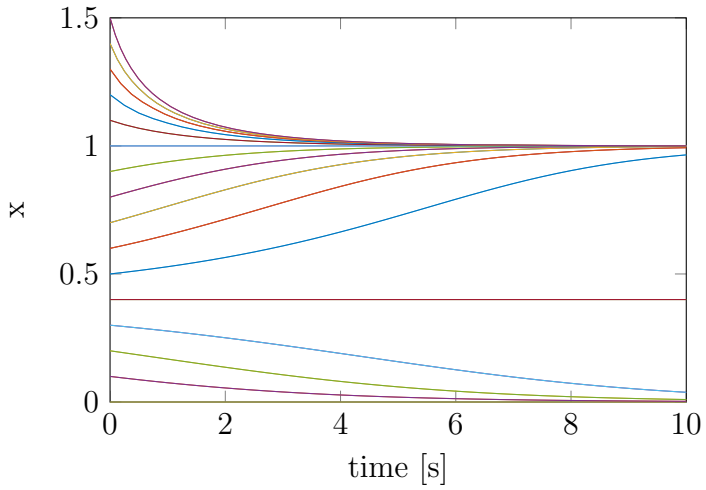

Figure 4.1: Simulation of the simplified system described by equation 4.3.

4.2.2 Two-dimensional approach

Once more the analysis starts with the computation of the fixed point locations. Setting the system equations to zero leads to:

$$0 = x(x-a)(1-x) - bxy \tag{4.8}$$
$$0 = xy - cy. \tag{4.9}$$

Starting from the top equation 4.8 first x may be factored out:

$$0 = x[(x-a)(1-x) - by]. \tag{4.10}$$

Therefore $x_1 = 0$. In order to obtain the remaining zeros the equation:

$$0 = (x-a)(1-x) - by \tag{4.11}$$

has to be solved. After factoring out the brackets the pq-Formula is applicable thus the following expression is obtained:

$$x_{2,3} = \frac{1+a}{2} \pm \sqrt{\frac{(1+a)^2}{4} - (a+by)}. \tag{4.12}$$

Which will be simplified further once more is known about y. To finish the quest for the fixed points x values y is factored out in the second equation:

$$0 = y(x-c). \tag{4.13}$$

The equation 4.13 is zero when $x_4 = c$. Which is the missing x component. Looking at y, $y_1 = 0$ is quickly read off from 4.13. Turning back to equation 4.8 and solving for y while assuming $x \neq 0$ gives:

$$y_2 = \frac{(c-a)(1-c)}{b} \tag{4.14}$$

$\mathbf{x}_1^* = \begin{pmatrix} x_1 \\ y_1 \end{pmatrix} = \begin{pmatrix} 0 \\ 0 \end{pmatrix}$
$\mathbf{x}_2^* = \begin{pmatrix} x_4 \\ y_2 \end{pmatrix} = \begin{pmatrix} c \\ \frac{(c-a)(1-c)}{b} \end{pmatrix}$
$\mathbf{x}_3^* = \begin{pmatrix} x_2 \\ y_1 \end{pmatrix} = \begin{pmatrix} 1 \\ 0 \end{pmatrix}$
$\mathbf{x}_4^* = \begin{pmatrix} x_3 \\ y_1 \end{pmatrix} = \begin{pmatrix} a \\ 0 \end{pmatrix}$

Table 4.1: Fixed point positions.

At this point two steady state solutions at $\begin{pmatrix} x_1 & y_1 \end{pmatrix}^T = \begin{pmatrix} 0 & 0 \end{pmatrix}^T$ and $\begin{pmatrix} x_4 & y_2 \end{pmatrix}^T = \begin{pmatrix} c & \frac{(c-a)(1-c)}{b} \end{pmatrix}^T$ are already known. Using y_1 again equation 4.12 can be simplified further after plugging in and factoring out one obtains:

$$x_{2/3} = \frac{1+a}{2} \pm \sqrt{\frac{1-2a+a^2}{4}} \tag{4.15}$$

$$x_{2/3} = \frac{1+a}{2} \pm \sqrt{(\frac{1-a}{2})^2} \tag{4.16}$$

$$x_{2/3} = \frac{1+a}{2} \pm \frac{1-a}{2} \tag{4.17}$$

$$\Rightarrow x_2 = 1 \wedge x_3 = a \tag{4.18}$$

Now two more fixed points are known $\begin{pmatrix} x_2 & y_1 \end{pmatrix}^T = \begin{pmatrix} 1 & 0 \end{pmatrix}^T$ and $\begin{pmatrix} x_3 & y_1 \end{pmatrix}^T = \begin{pmatrix} a & 0 \end{pmatrix}^T$.

Next the obtained points will be classified according to their properties. Starting from the system equations after factoring out the Jacobian is computed:

$$J = \begin{pmatrix} -3x^2 + 2x + 2xa - a - yb & -bx \\ y & x - c \end{pmatrix} \tag{4.19}$$

Linear analysis proceeds by plugging the fixed points into the Jacobian and compute the trace τ as well as the determinant $\triangle$. For the first fixed point $\mathbf{x}_1^*$ this gives:

$$J(\mathbf{x}_1^*) = \begin{pmatrix} -a & 0 \\ 0 & -c \end{pmatrix}. \tag{4.20}$$

Therefore the trace and determinant are $\tau_1 = -a - c \wedge \triangle_1 = ac$. Thus this node is a saddle point if $c < 0$, if $c > 0$ it is stable if $-a < c$. The spiral condition $\tau_1 - 4\triangle = (a-c)^2 < 0$, therefore this point should never spiral. The second fixed point $\mathbf{x}_2^*$ has the Jacobian:

$$J(\mathbf{x_2^*}) = \begin{pmatrix} c(1+a-2c) & -bc \\ (c-a)(1-c)/b & 0 \end{pmatrix} \tag{4.21}$$

With the determinant and trace $\tau_2 = c(1+a-2c) \wedge \triangle_2 = c(c-a)(1-c)$. From these two expressions it is possible to deduce, that if $c > 0$, $\mathbf{x_2^*}$ is a saddle point if additionally, $c > a \wedge c < 1$. If that is not the case then the determinant is positive, now the trace determines stability. $\tau_2 < 0$ is the case if $\frac{1+a}{2} < c$. However it $c < 0$ then the determinant

	$c \in [0, 0.4]$	$c \in [0.4, 0.45]$	$c \in [0.45, 0.7]$	$c \in [0.7, 0.9]$	$c \in [0.9, 1]$	$c \in [1, 1.5]$
$\mathbf{x}_1^*$	stable node	stable node	stable node	stable node	stable node	stable node
$\mathbf{x}_2^*$	saddle point	unstable node	unstable spiral	stable spiral	stable node	saddle point
$\mathbf{x}_3^*$	saddle point	saddle point	saddle point	saddle point	saddle point	stable node
$\mathbf{x}_4^*$	unstable node	saddle point	saddle point	saddle point	saddle point	saddle point

Table 4.2: Fixed point classification for various intervals of c

will always be negative, making $\mathbf{x_2^*}$ a saddle point. If the third fixed point is plugged into the Jacobian-matrix it changes to:

$$J(\mathbf{x_3^*}) = \begin{pmatrix} -1+a & -b \\ 0 & 1-c \end{pmatrix} \tag{4.22}$$

This matrix has the trace $\tau_3 = -c + a$ and the determinant $\triangle_3 = (a-1)(1-c) = a - ac - 1 + c$. Therefore the determinant if positive if $c > 1$ assuming that $(1-a) > 0$, which is known to be true since $a = 0.4$. If the determinant is positive the node is stable if $\tau_3 < 0 \Rightarrow a < c$. The node has spirals is $\tau^2 - 4\triangle < 0$. All that remains is the Jacobian of the fourth fixed point:

$$J(\mathbf{x_4^*}) = \begin{pmatrix} -a^2+a & -ba \\ 0 & a-c \end{pmatrix} \tag{4.23}$$

$\tau_4 = a^2 + 2a - c$, $\triangle_4 = (-a^2 + a)(a - c) = -a^3 + a^2c + a^2 - ac$.

Topological analysis

In this section the topology of the first interval $c \in [0, 0.4]$ will be deduced from the eigenvalues and eigenvectors. For $\mathbf{x}_1^*$ reading off from 4.20 the eigenvalues are found to be:

$$\lambda_{1,1} = -a \tag{4.24}$$
$$\lambda_{1,2} = -c \tag{4.25}$$

with the eigenvectors:

$$\mathbf{v}_{1,1} = \begin{pmatrix} 1 & 0 \end{pmatrix}^T \tag{4.26}$$
$$\mathbf{v}_{1,2} = \begin{pmatrix} 0 & 1 \end{pmatrix}^T \tag{4.27}$$

Thus around the stable node $(1, 1)$ all trajectories are drawn towards this stable node.

For $\mathbf{x}_2^*$ no general expressions could be found from 4.21, the ones given are for $c = 0.2, a = 0.4$ and $b = 0.3$:

$$\lambda_{2,1} = 0.305 \tag{4.28}$$
$$\lambda_{2,2} = -1.04 \tag{4.29}$$
$$\mathbf{v}_{2,1} = \begin{pmatrix} -0.571 & 1 \end{pmatrix}^T \tag{4.30}$$
$$\mathbf{v}_{2,2} = \begin{pmatrix} 0.1967 & 1 \end{pmatrix}^T. \tag{4.31}$$

We have an unstable eigenvalue, therefore from this node the trajectories will leave along $\pm\mathbf{v}_{2,1}$ towards zero and infinity. While $\pm\mathbf{v}_{2,2}$ guides orbits toward the node.

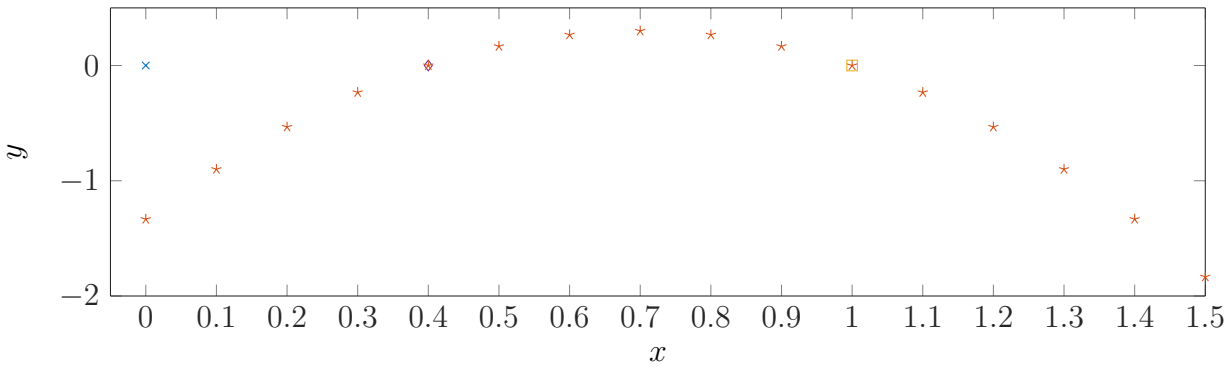

Figure 4.2: Fixed point position for varying c. The constant position of $\mathbf{x}_1^*$ is marked with an x at $0, 0$. The variable position of $\mathbf{x}_2^*$ is marked with a series of stars. Finally $\mathbf{x}_3^*$ and $\mathbf{x}_4^*$ are always at $0.4, 0$ and $1, 0$ marked with a square and a diamond.

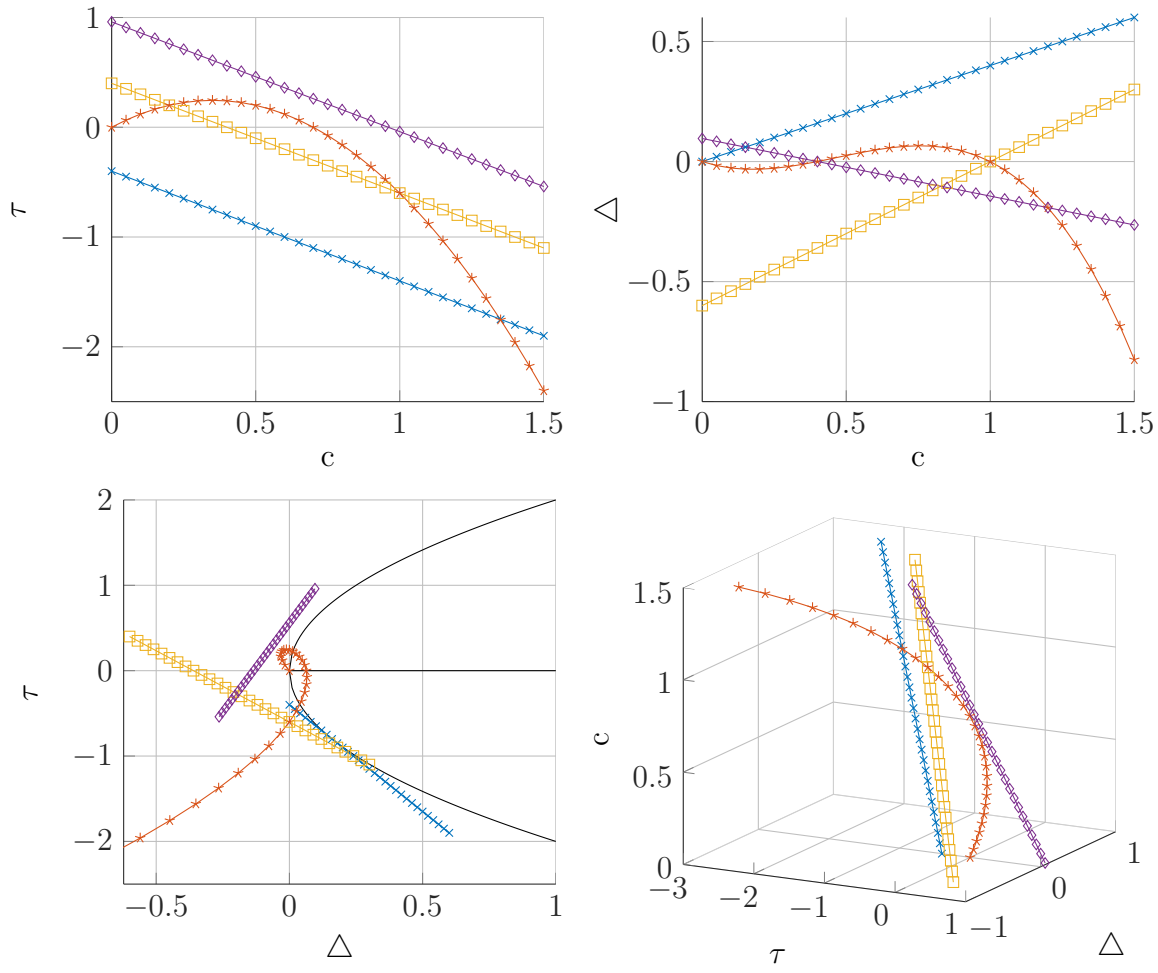

Figure 4.3: Jacobian trace and determinant for the four fixed points for increasing c. Values associated with $\mathbf{x}_1^*$ are marked with an x and shown in blue. Plots connected to $\mathbf{x}_2^*$ are marked with stars and graphed in orange. Representations of the trace and determinant of $\mathbf{x}_3^*$ have squares on each line and are colored in yellow. Finally values connected to $\mathbf{x}_4^*$ are marked with a diamonds and a drawn in purple.

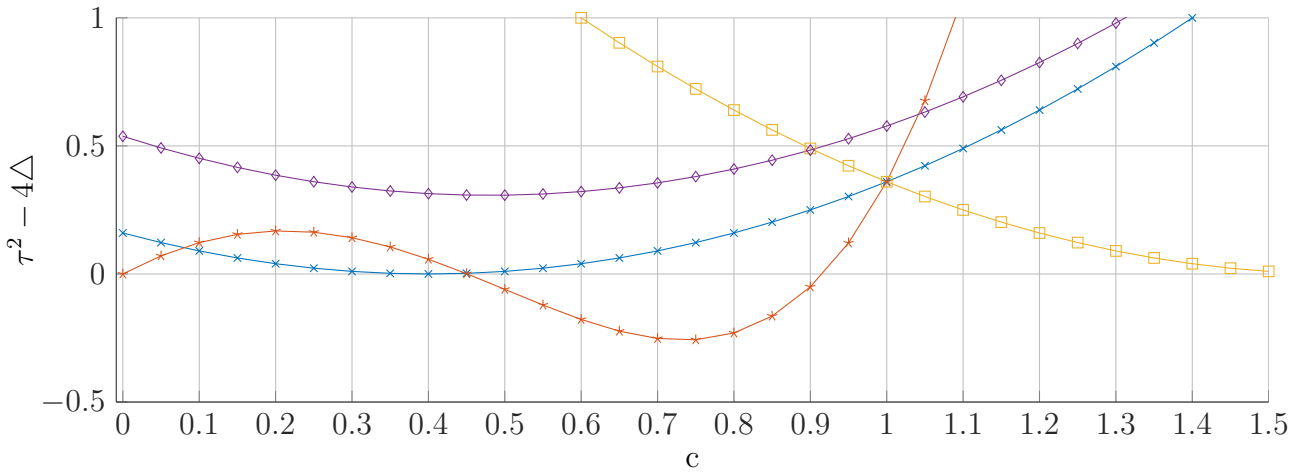

Figure 4.4: Plot of the spiral condition for all four fixed points. If $\tau^2 - 4\triangle < 0$ a node turns into a spiral.

For $\mathbf{x}_3^*$ the eignevalues of the Jacobian 4.22 may be read of the diagonal:

$$\lambda_{3,1} = -1 + a \tag{4.32}$$
$$\lambda_{3,2} = 1 - c. \tag{4.33}$$

With the eigenvalues known the eigenvectors may be computed, they turn out to be:

$$\mathbf{v}_{3,1} = \begin{pmatrix} 1 & 0 \end{pmatrix}^T \tag{4.34}$$
$$\mathbf{v}_{3,2} = \begin{pmatrix} \frac{b}{-2+a+c} & 1 \end{pmatrix}^T. \tag{4.35}$$

When a, b, c are replaced with their numerical values this leads to $\lambda_{3,1} = -0.6$, and $\lambda_{3,2} = 0.8$. Similarly for the eigenvectors, $\mathbf{v}_{3,1} = \begin{pmatrix} 1 & 0 \end{pmatrix}^T, \mathbf{v}_{3,2} = \begin{pmatrix} -2.1428 & 1 \end{pmatrix}^T$ is obtained.

Finally for $\mathbf{x}_4^*$ is very similar from 4.23;

$$\lambda_{4,1} = -a^2 + a \tag{4.36}$$
$$\lambda_{4,2} = a - c, \tag{4.37}$$

are the read off eigenvalues, thus the eigenvectors are:

$$\mathbf{v}_{4,1} = \begin{pmatrix} 1 & 0 \end{pmatrix}^T \tag{4.38}$$
$$\mathbf{v}_{4,2} = \begin{pmatrix} \frac{-ab}{a^2-c} & 1 \end{pmatrix}^T \tag{4.39}$$

One last time the numerical values have to be fed into the expressions, this yields $\lambda_1 = 0.24$ and $\lambda_2 = 0.2$. And for the vectors, $\mathbf{v}_{4,1} = \begin{pmatrix} 1 & 0 \end{pmatrix}^T, \mathbf{v}_{4,2} = \begin{pmatrix} 3 & 1 \end{pmatrix}^T$. At this point numerical values for all eigenvalue, eigenvector pairs are known. If the eigenvectors are added and subtracted from their corresponding fixed points location. The image shown in figure 4.5 is obtained. It is important to note that most eigenvectors have been scaled by either six or three to address scaling problems. The eigendirection has been deduced from the eigenvalues. $\lambda > 0$ means unstable $\lambda < 0$ means stable or attracting.

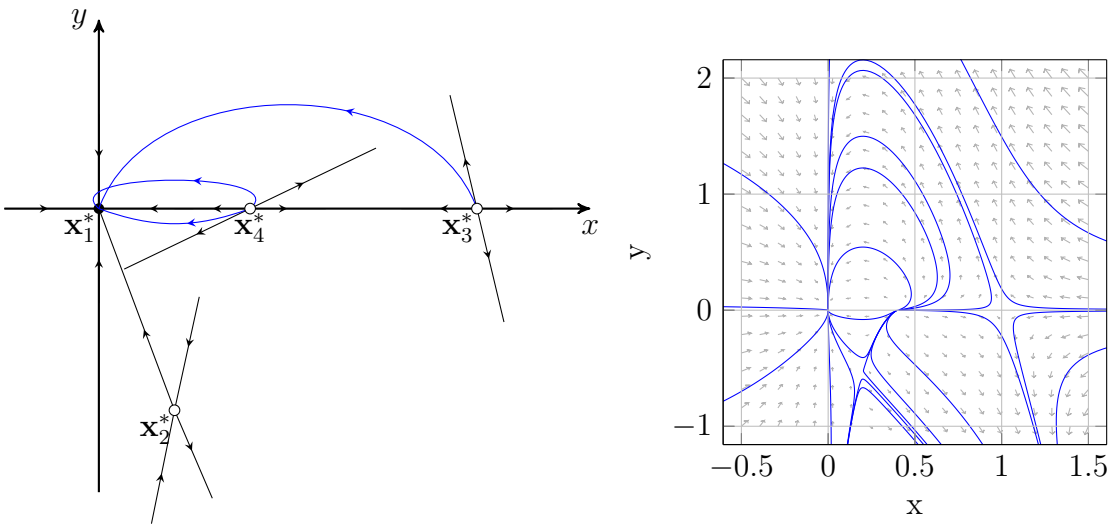

Figure 4.5: Prediction of the topology of the predator prey model for $c = 0.2$. Eigenvector based predictions are shown in black, others in blue (left). Numerical simulation results using `pplane` for the same set of parameters (right).

4.2.3 Numerical Analysis

In order to fully graph the topology the topological analysis outlined above for $c = 0.2$ would have to be repeated five times. As this is a very tedious and error prone endeavor pplane will be used instead. Results are shown in figure 4.7. A quick comparison with table 4.2 and figure 4.2 confirms the predictions made earlier. When c is chosen greater then 0.7, two attracting nodes will exist. Which raises the question, which areas of the phase plane will be attracted to which attractor. The separatrices which separate these areas are the answer to this question. These lines are trajectories, that run along the border of the basins of attraction of two different attractors separating them. Typically these trajectories end at a saddle point [1]. For $c > 0.7$ $\mathbf{x}_4^*$ remains a saddle point at all times. Furthermore it lies between the stable nodes, for which the basin of attraction is to be determined. The stable eigenvectors of $\mathbf{x}_4^*$ are thus likely to point along the separatrices. $\mathbf{x}_4^*$ is located at:

$$\mathbf{x}_4^* = \begin{pmatrix} a \\ 0 \end{pmatrix} = \begin{pmatrix} 0.4 \\ 0 \end{pmatrix} \tag{4.40}$$

From equations 4.37 and 4.39 the stable eigenvector is determined to be:

$$\mathbf{v}_{4,2} = \begin{pmatrix} \frac{-ab}{a^2-c} \\ 1 \end{pmatrix} = \begin{pmatrix} 0.1875 \\ 1 \end{pmatrix} \tag{4.41}$$

Thus one would expect a separatrice that is pointing upwards ($y = 1$) and slightly to the right ($x = 0.1875$). If the eigenvector found above is added and subtracted from $\mathbf{x}_4^*$ figure 4.6 is obtained. Here the stable and unstable manifolds meet. The situation depicted comes form the one for $c = 0.8$ in figure 4.7 here only the top separatrices is drawn in red, however the idealization drawn earlier turns out to be true around $\mathbf{x}_4^*$.

[1] Strogatz p.158

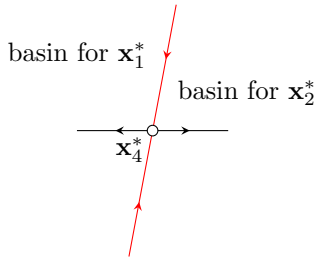

Figure 4.6: Idealized depiction of the separatrices at $\mathbf{x}_4^*$

4.3 Bifurcation Analysis

Figure 4.8 shows the evolution of the real and imaginary part of $J(\mathbf{x}_2^*)$'s two eigenvalues. Originally both eigenvalues are real with one being positive and one negative. Therefore $\mathbf{x}_2^*$ is initially a saddle point. The situation changes when the second eigenvalues becomes positive. The node now turns into an unstable one. When the eigenvalues' imaginary parts start to have nonzero values spiraling will start to occur. With the spirals stability determined by the real parts. At 0.7 the both real parts turn negative causing a reverse Hopf-bifurcation[2] which ultimately results in stable spiral. When the eigenvalues turn real again at 0.9 the spiraling stops and a stable node is created. Finally as the real parts take opposing signs $\mathbf{x}_2^*$ turns into a saddle point again, just like it was in the beginning.

As c increases from 0.65 to 0.75 , most importantly at 0.7 the reverse Hopf-bifurcation occurs. For $c = 0.7$ initial conditions close the the fixed points $\mathbf{x}_2^*$ will keep oscillating almost undamped see figures 4.9 and 4.7 . The period of the solutions decreases as orbits come closer to the separatrice, which can be observed in figure 4.9. Perhaps not very surprisingly before the bifurcation both species die out as the node at $(0, 0)$ is the only fixed point, that can be reached from positive initial conditions. At $c = 0.7$ the two animal races have at least the option of eternal oscillation instead of mutual extinction. Finally after the bifurcation all three initial conditions tried out here converge to the stable spiral at $\mathbf{x}_2^*$. However it is important that $\mathbf{x}_1^*$ at $(0, 0)$ remains stable and is indeed approached from other initial conditions. Figures 4.10 and 4.11 show bifurcation diagrams for $d = 0$, $d = 0.01$ and finally $d = -0.01$. For the $d = 0$ case `matcont` correctly detects the Hopf-bifurcation, that was already identified from the eigenvalues. Additionally it marks the points where $\mathbf{x}_2^*$ changes its stability as branch points. The parameter d changes the nature of the bifurcations drastically like an imperfection parameter it introduces symmetric distortions with respect to the sign of d.

[2]Strogatz p.252

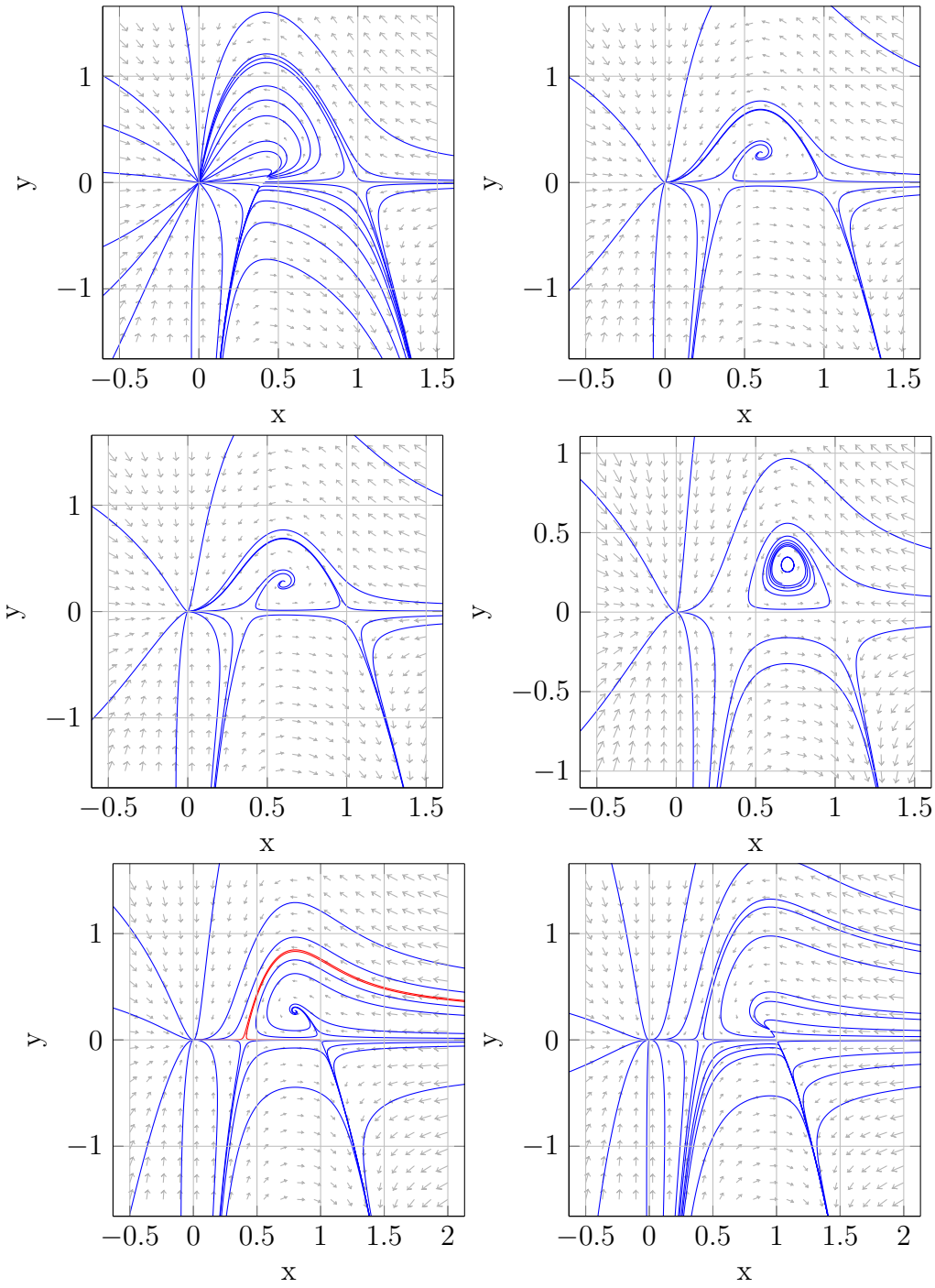

Figure 4.7: Phase plane topology found by `pplane` for $c = 0.425, 0.6, 0.7, 0.8, 0.95$. In the plot for $c = 0.8$ the separatrices have been drawn in red.

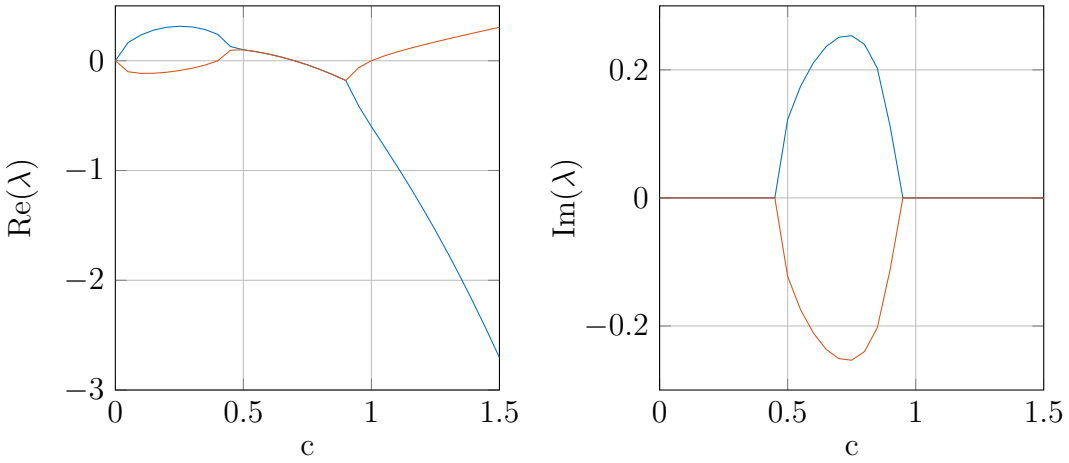

Figure 4.8: Evolution of real and complex part of $\texttt{eig}(J(\mathbf{x}_2^*))$

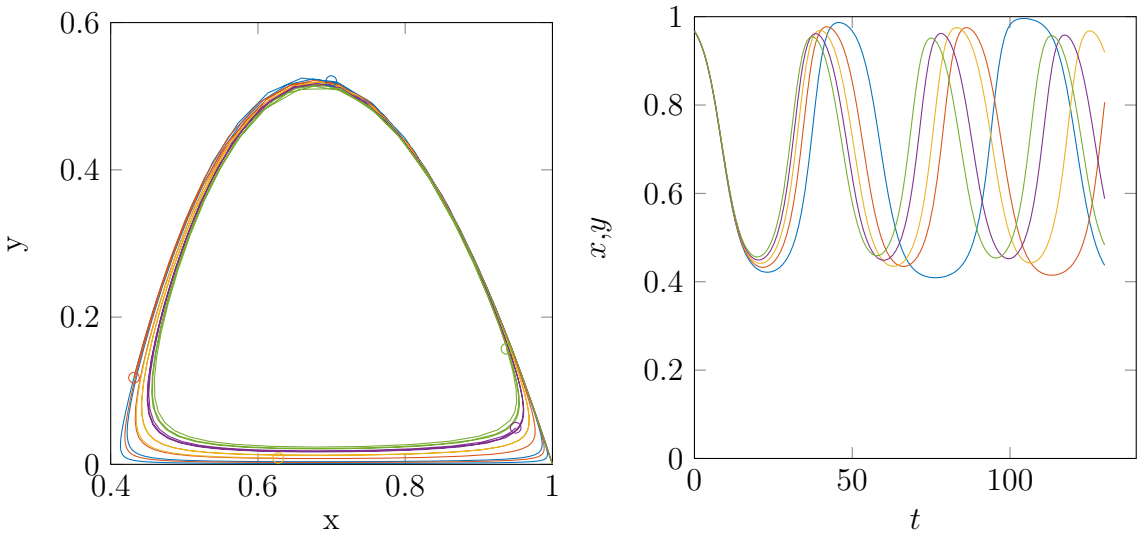

Figure 4.9: System solutions for $c = 0.677, 0.678, 0.679, 0.68, 0.681$ in time and phase plane representation.

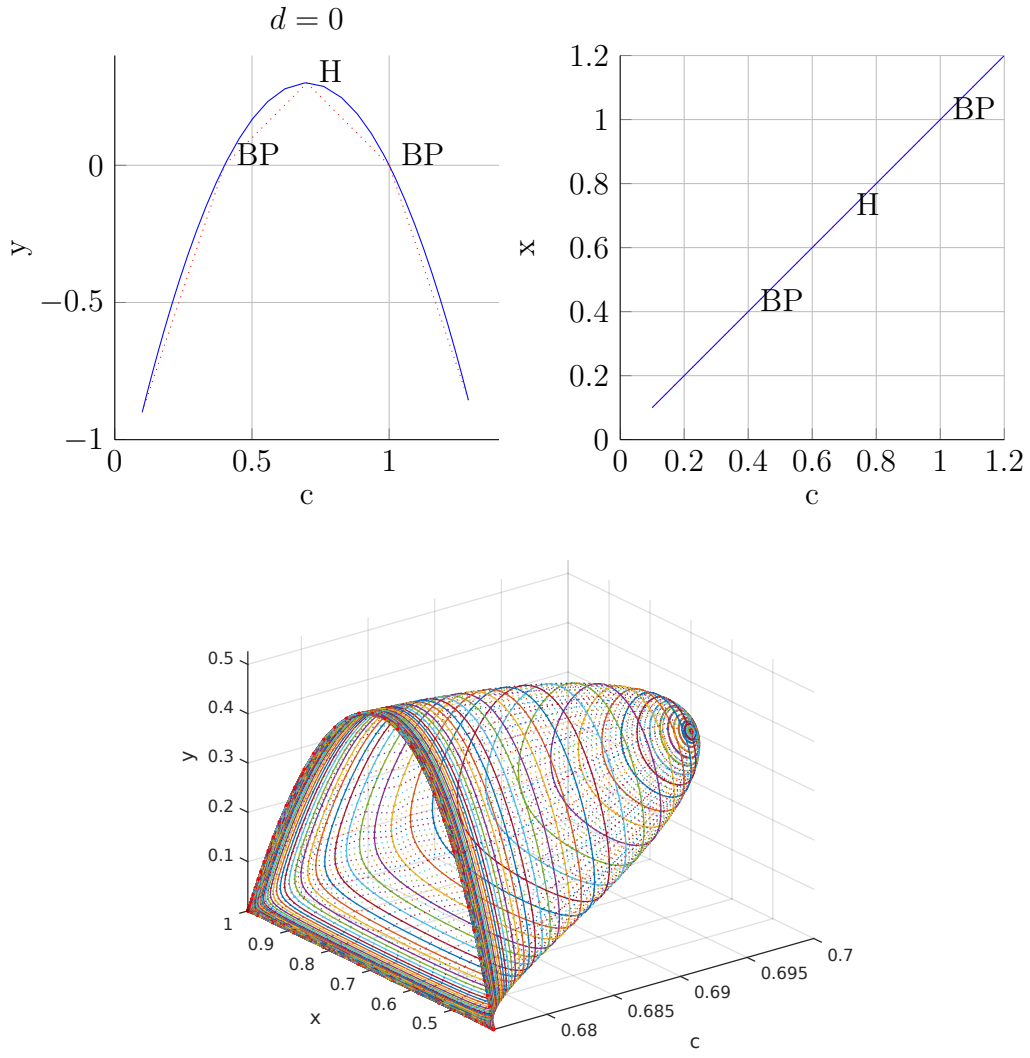

Figure 4.10: `matcont` continuation for $\mathbf{x}_2^*$ starting from $c = 0.1$ as projection on x, c and y, c. Limit cycle continuation troughout its short lifetime.

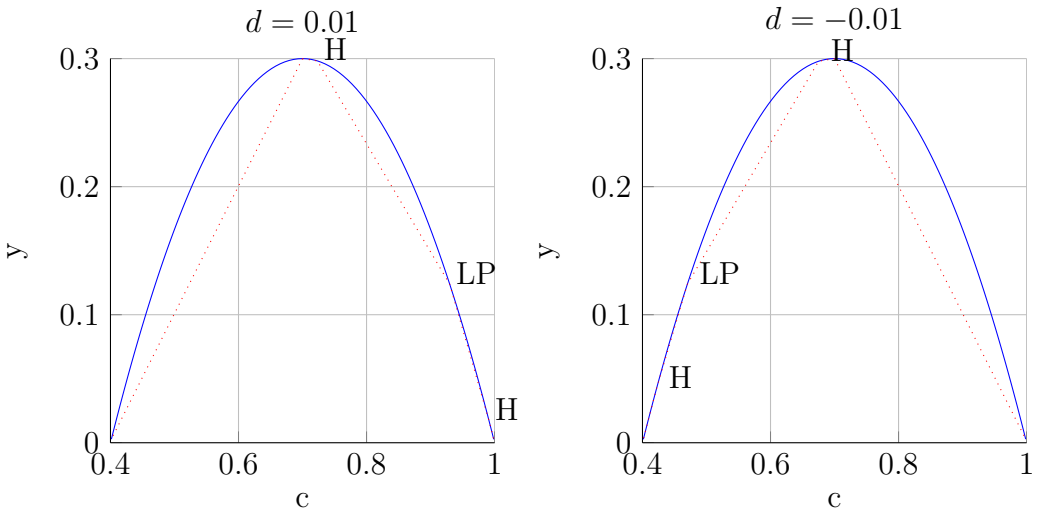

Figure 4.11: `matcont` made bifurcation diagrams. With $d = 0.01$ and $d = -0.01$

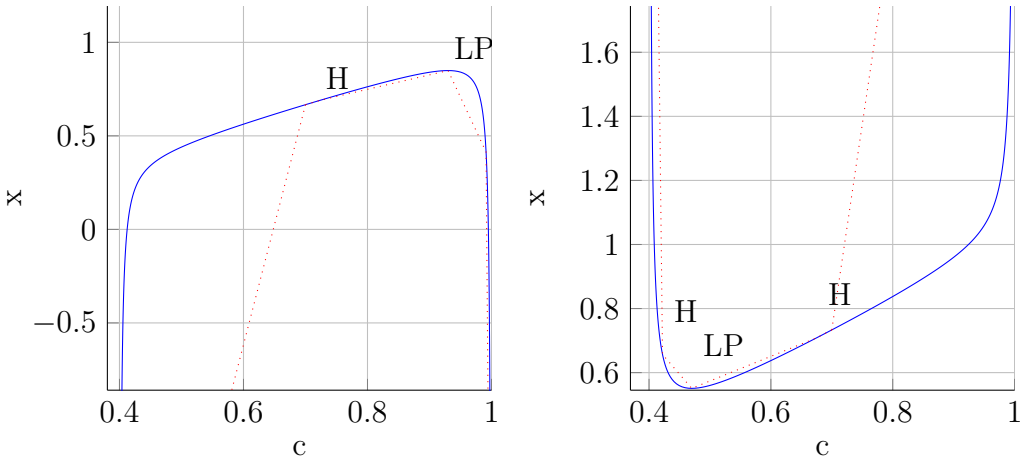

Figure 4.12: `matcont` made bifurcation diagrams. With $d = 0.01$ and $d = -0.01$, in c, x projection.

Chapter 5

Chaos

5.1 Lyapunov exponents of the Lorenz equations

The Lorenz-equations are considered chaotic as they exhibit sensitive dependence on initial conditions. An important way to put this dependence into numbers are Lyapunov exponents. If the evolution of the distance between the solutions starting from two initial conditions $\delta(t)$ is compared. The biggest Lyapunov exponents tells us how this distance will change with time[1]:

$$\|\delta(t)\| \sim \|\delta_0\| e^{\lambda t} \tag{5.1}$$

This means that a system with at least one positive Lyapunov exponent will become unpredictable after a certain time horizon is reached. This behavior can be observed in figure 5.1. The one of the four solutions spread out on the attractor even tough their initial conditions where only 0.1 apart. Conceptually the exponents are computed following the formula [2]:

$$\lambda = \lim_{n\to\infty} \{\frac{1}{n} \sum_{i=0}^{n-1} \ln(f'(x_i)\} \tag{5.2}$$

However instead of the first derivative the Jacobian matrix is computed. The rows, which contain the spacial derivatives at a given point x_i of a given equation. In order to produce a scalar the square root of the dot product is computed for the row under consideration and then fed into the logarithm. Generally one obtains as many exponents as equations. In order to prevent nasty numerical surprises the rows of the Jacobian are kept orthogonal by the Gram-Schmidt algorithm.

To undertake numerical computations it is necessary to choose a value `kkmax` $< \infty$ as a replacement for n. Furthermore a step size `st` is necessary. The time covered by the simulation would therefore be `st * kkmax`. When starting the computation three input-parameters are at the users disposal. At first a suitable initial condition has to be chosen. In order to avoid any traveling time where the solutions move onto the attractor (see figure 5.1) the initial condition `[0 1 20]` has been chosen, which is on or very close to the attractor. Next step size and the number of iterations have to be picked. As an initial gees `st = 0.01; kkmax = 1000` are proposed. The results are shown in figure5.2. If only the number of iterations is increased it remains debatable if the solution quality

[1] Strogatz p.328
[2] Strogatz p.374

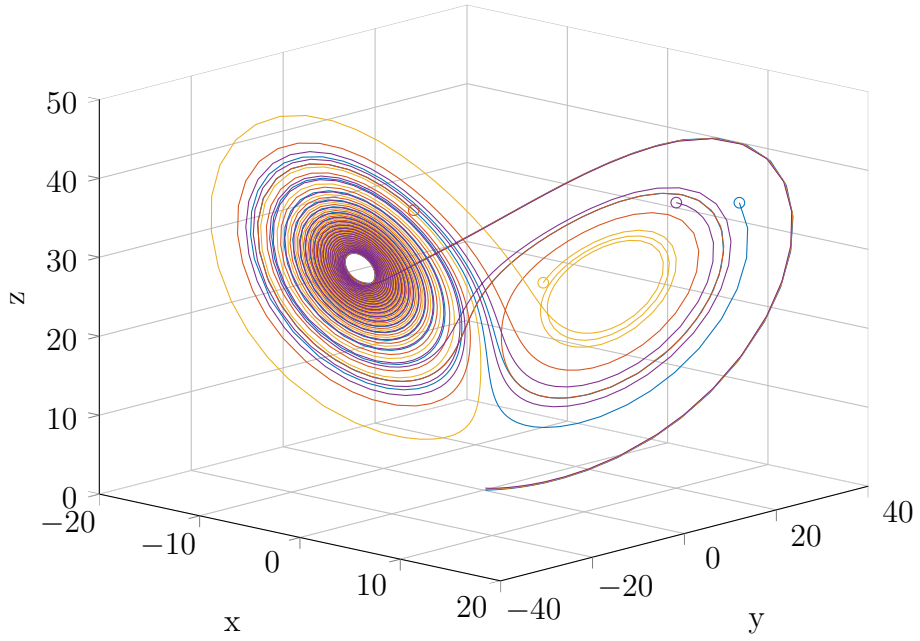

Figure 5.1: Numerical solution of the Lorenz equations for the four initial conditions $(0.2, 0, 0), (0.2, 0, 0.1), (0.2, 0, 0.2), (0.2, 0, 0.3)$ for $t \in [0, 20]$. Solution end points are marked with circles.

actually increases. See figure 5.3. However if the step size is reduced by the same order of magnitude with which the number of iterations was increased, the solution precision does indeed improve. Check figure 5.4.

5.2 The duffing Oscillator

$$\ddot{x} + k\dot{x} + x^3 = B\cos(t). \tag{5.3}$$

In Ueda's 1980 paper on "Steady Motions exhibited by Duffing's Equation" [3], the dynamics of equation 5.3 is analyzed for numerous different k and B value combinations. In this report the combination `k = 1; B = 5` which should lead to stable results, will be compared to `B = 7.5;k = 0.05`, which is supposed to produce chaotic results. Results are shown in figures 5.5 and 5.6. As predicted in the paper chaotic behaviour does occur for the second parameter set. The initial conditions which are only 0.1 apart end up on completely different parts of the oscillator. A result that differs fundamentally from the behavior induced by the first parameter set. In this case the solutions are attracted to one stable path in the oscillator.

5.3 Chua's circuit

One last example of chaos is Chua's circuit. As the name hints it stems from circuit theory. Once more four sightly perturbed initial conditions are simulated, results are shown in figure 5.8. The Lyapunov exponents are found to be `lyap = 0.3123 0.1702`

[3] http://www.iaea.org/inis/collection/NCLCollectionStore/_Public/12/574/12574072.pdf

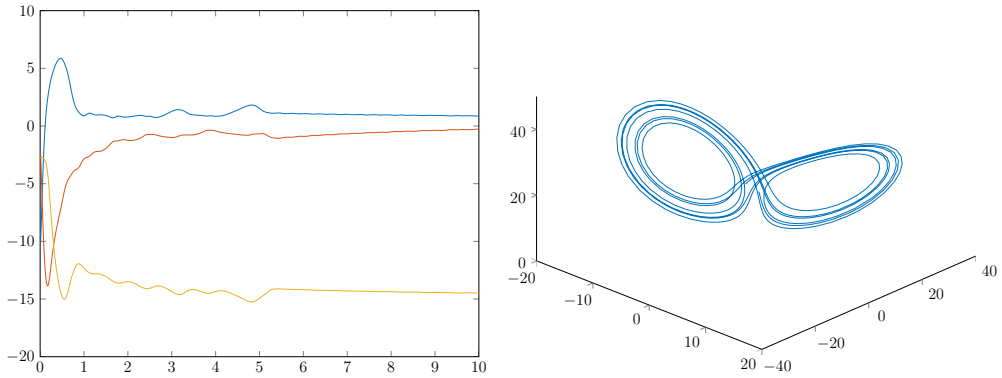

Figure 5.2: `x = [0 1 20]'; st = 0.01; kkmax = 1000; lyap = 0.8512 -0.2526 -14.4998`

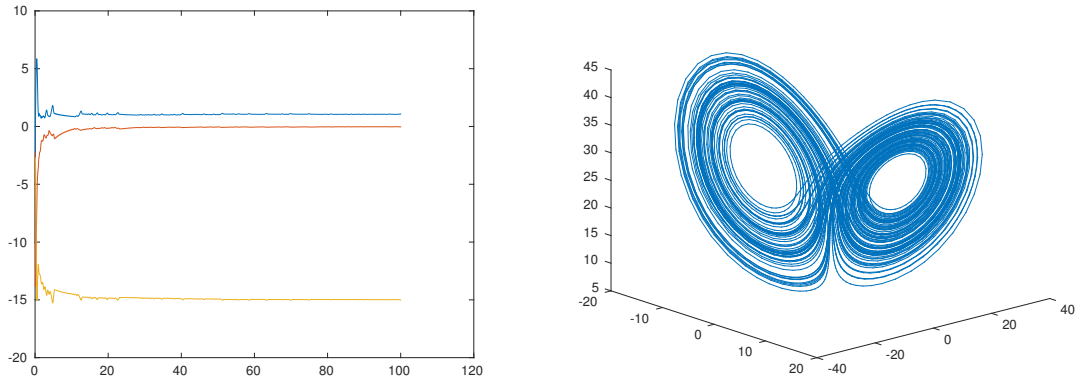

Figure 5.3: `x = [0 1 20]';st = 0.01;kkmax = 10000; lyap = 1.0749 -0.0312 -14.9990`

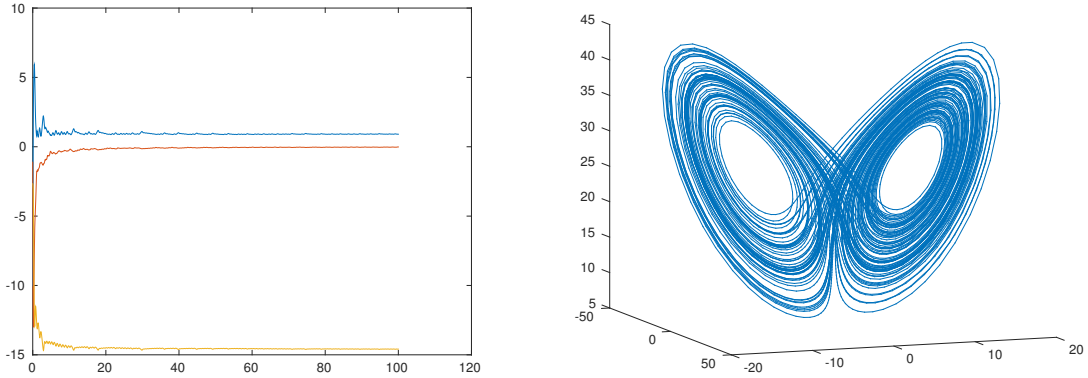

Figure 5.4: `x = [0 1 20]'; st = 0.001; kkmax = 100000; lyap = 0.9035 -0.0150 -14.5896`

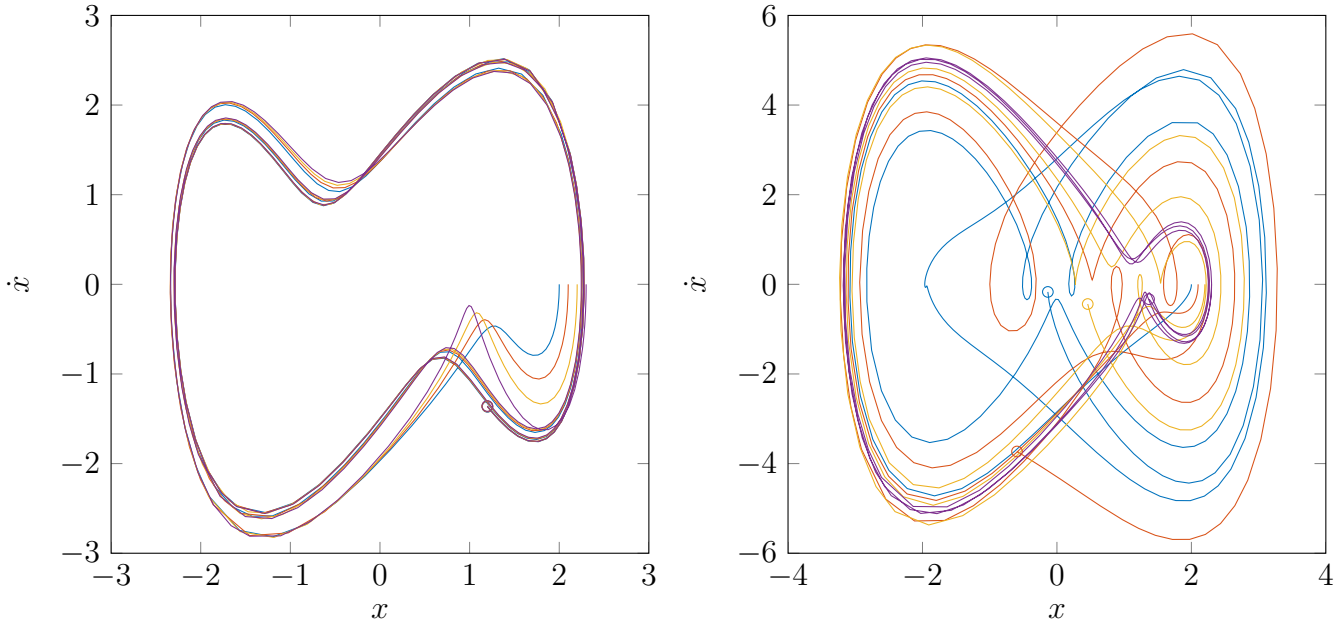

Figure 5.5: Stable Duffing-oscillator with `k = 1; B = 5`. Slightly perturbed initial conditions end up on the same path eventually (left). Chaotic Duffing-oscillator with `B = 7.5;k = 0.05`. Slightly perturbed initial conditions end up on different parts of the oscillator.

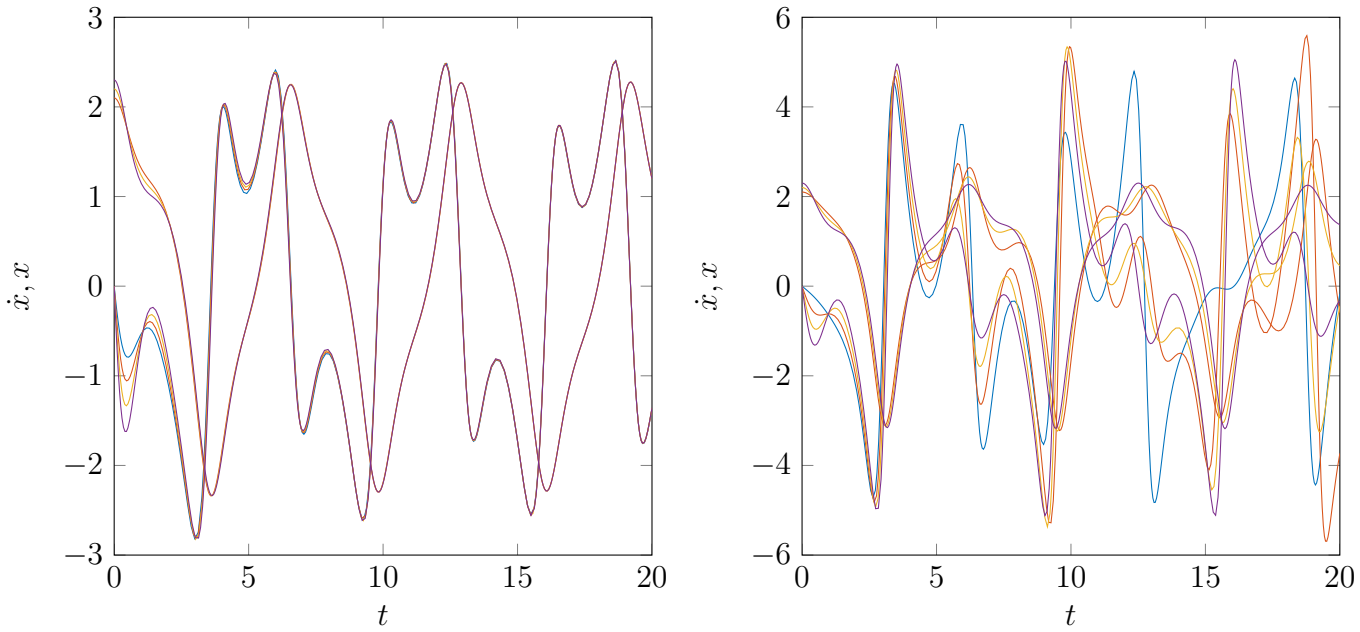

Figure 5.6: Time plot of the duffing oscillator's first and second derivative. For `k = 1; B = 5`(left) and `B = 7.5;k = 0.05`(right).

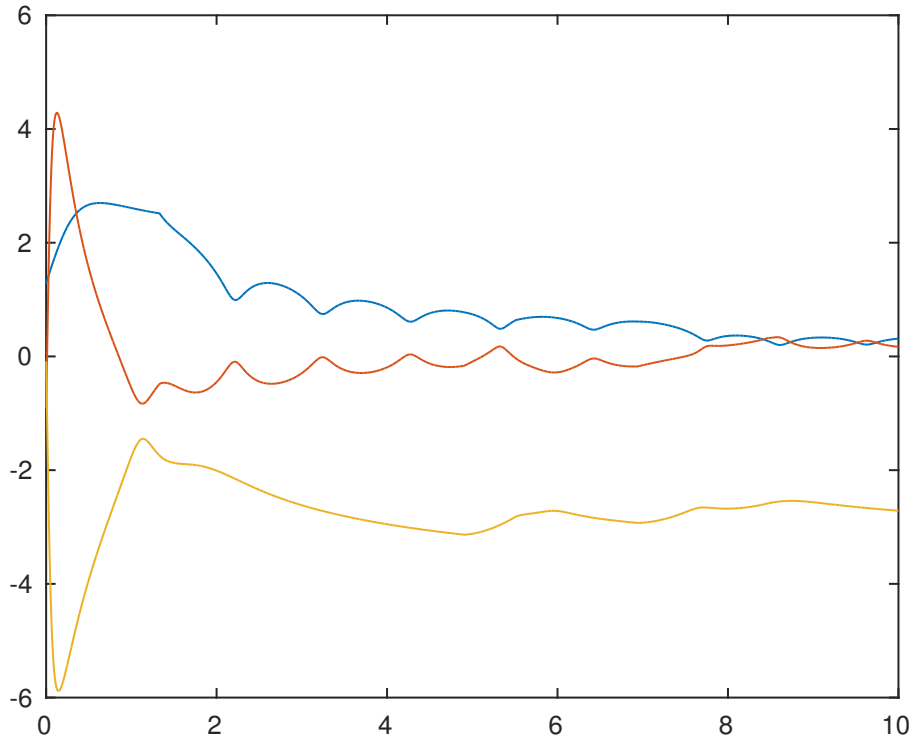

Figure 5.7: Evolution of the Liapunov exponents during first iterations of the Jacobian based algorithm.

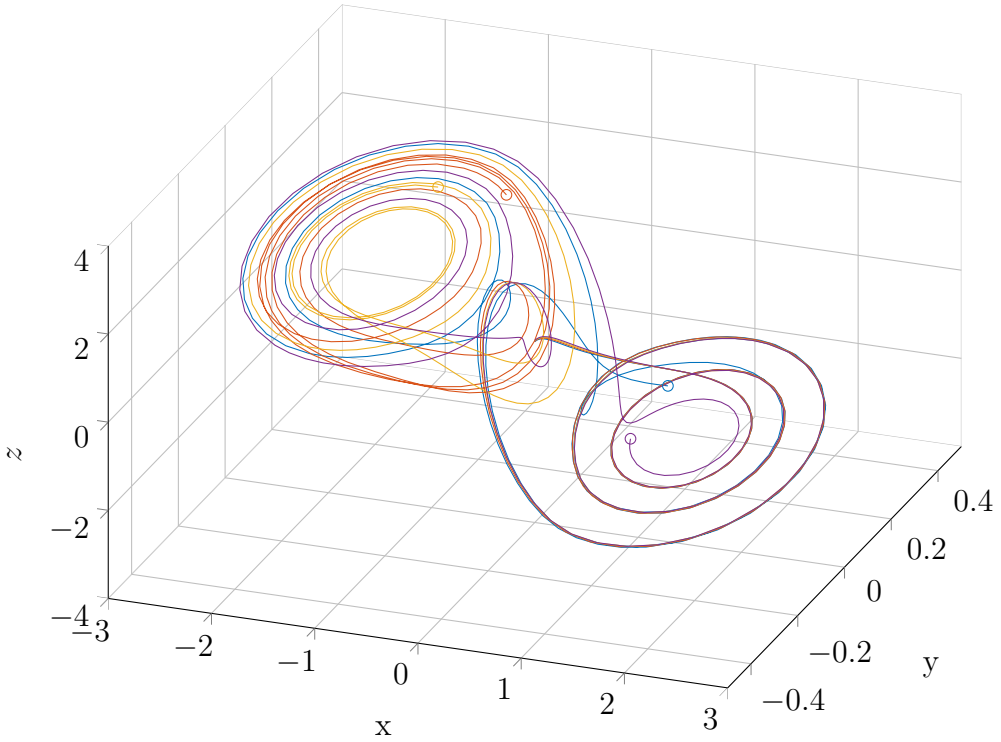

Figure 5.8: Simulation of Chua's circuit starting from $\mathbf{x}_{1,0} = (0, 0, 0.1)$, $\mathbf{x}_{2,0} = \mathbf{x}_{1,0} \cdot 1.1$, $\mathbf{x}_{3,0} = \mathbf{x}_{1,0} \cdot 1.2$ and $\mathbf{x}_{4,0} = \mathbf{x}_{1,0} \cdot 1.3$, `lyap = 0.3123 0.1702 -2.7140`.

-2.7140, with two exponents greater then zero indicating chaotic behavior. A prediction that is confirmed by the observation of perturbation sensitivity in the computed orbits.

Chapter 6

Pattern formation

6.1 The Brusselator

$$u_t = D_u u_{xx} + A - (B+1)u + u^2 v, \tag{6.1}$$
$$v_t = D_v v_{xx} + Bu - u^2. \tag{6.2}$$

The above equations describe molecule concentrations during a coupled reaction. They are known to exhibit patterns.

6.2 Stability of the steady state

At the steady state $u_t = v_t = u_{xx} = v_{xx} = 0$. Thus following equations remain:

$$0 = A - (B+1)u + u^2 v, \tag{6.3}$$
$$0 = u(B - uv). \tag{6.4}$$
$$\tag{6.5}$$

From which $u_0 = A$ and $v_0 = B/A$ is deduced. Considering the linearized system evaluated at u_0,v_0 in Matrix form:

$$\begin{pmatrix} u_t \\ v_t \end{pmatrix} = \begin{pmatrix} D_u u_{xx} \\ D_v v_{xx} \end{pmatrix} + \underbrace{\begin{pmatrix} B-1 & A^2 \\ -B & -A^2 \end{pmatrix}}_{\text{Jacobian evaluated at } (u_0, v_0)} \begin{pmatrix} u \\ v \end{pmatrix}. \tag{6.6}$$

From the Jacobian above trace and determinant of the ordinariy differential subsystem can be read off, $\tau_{ode} = B-1-A^2$ and $\triangle_{ode} = A^2$. Using $\begin{pmatrix} u & v \end{pmatrix}^T = \begin{pmatrix} u_1 & v_1 \end{pmatrix}^T \cdot \exp(\lambda t + ikx)$ leads to:

$$u_{xx} = (ik)^2 u_1 \exp(st + ikx) = -k^2 u \tag{6.7}$$
$$u_{yy} = (ik)^2 v_1 \exp(st + ikx) = -k^2 v \tag{6.8}$$

When substituting this into the linearized equation 6.6. The expression:

$$\begin{pmatrix} u_t \\ v_t \end{pmatrix} = \begin{pmatrix} (B-1) - k^2 D_u & A^2 \\ -B & -A^2 - k^2 D_v \end{pmatrix} \begin{pmatrix} u \\ v \end{pmatrix}. \tag{6.9}$$

The new matrix above has trace τ and determinant $\triangle$:

$$\tau = B - 1 - A^2 - k^2(D_u + D_v) \tag{6.10}$$
$$\triangle = [(B-1) - k^2 D_u][-A^2 - k^2 D_v] + BA^2 \tag{6.11}$$
$$= A^2 - BA^2 + A^2k^2D_u + k^2D_vB - k^2D_v + k^2D_uD_v + BA^2 \tag{6.12}$$
$$= A^2 + k^2(A^2D_u + (1-B)D_v) + k^4D_uD_v. \tag{6.13}$$

Now linear algebra has a nice relationship for the eigenvalues:

$$\lambda_\pm = \frac{1}{2}(\tau \pm \sqrt{\tau^2 - 4\triangle}). \tag{6.14}$$

6.3 Turing instability

Turing instability can occur when the ordinary differential and the partial differential part of the system work against each other. Or in other terms it instability is requires:

$$\tau_{ode} < 0 \wedge \triangle_{ode} > 0 \tag{6.15}$$
$$(\tau_{pde} > 0 \wedge \triangle_{pde} > 0) \vee \triangle_{pde} < 0. \tag{6.16}$$

Where the subscripted τ_{ode} and $\triangle_{ode}$ denote trace and determinant of the ordinary differential system and τ_{pde} and $\triangle_{pde}$ trace and determinant of the partial differential part. When real eigenvalues of the partial differential subsystem change sign, the onset of Turing instability is observed. That is because the determinant which is the product of the two eigenvalues will change it's sign if any of the eigenvalues do. If both pde system eigenvalues change sign with respect to the ode system, τ_{pde} changes it's sign instead of $\triangle_{pde}$.

Using the conditions outlined above a critical value for B may be computed, looking at the inequalities for the ordinary part:

$$\tau_{ode} = B - 1 - A^2 < 0 \Leftrightarrow B < 1 + A^2 \tag{6.17}$$
$$\triangle_{ode} = A^2 > 0. \tag{6.18}$$

The two inequalities have to be respected, when creating an turing unstable Brusselator. Starting from $\triangle_{pde} = 0$. A critical value for an increasing B is sought after in the upcoming part:

$$0 = A^2 + k^2(A^2D_u + (1-B)D_v) + k^4D_uD_v \tag{6.19}$$
$$B = \frac{A^2D_u}{D_v} + 1 + \frac{A^2}{k^2D_v} + k^2D_u. \tag{6.20}$$

However to evaluate the expression above a value for the variable k is required. As the goal of this train of thought is to find the smallest B for which instability occurs, k hast to be chosen such that it minimizes B. This can be done by solving $\frac{dB}{dk} = 0$ and later

checking that $\frac{d^2B}{dk^2} > 0$ to verify a minimum. The first derivative is given by:

$$0 = -\frac{2A^2}{k^3 D_v} + 2kD_u \tag{6.21}$$

$$\Leftrightarrow 2A^2 = 2k^4 D_u D_v \tag{6.22}$$

$$\Leftrightarrow k^4 = \frac{A^2}{D_u D_v} \tag{6.23}$$

$$\Leftrightarrow k_T = (\frac{A^2}{D_u D_v})^{\frac{1}{4}}. \tag{6.24}$$

The second derivative is described by:

$$\frac{d^2B}{dk^2} = \frac{6A^2}{k^4 D_v} + 2D_u \tag{6.25}$$

Substituting k_T into 6.25 yields:

$$\frac{d^2B}{dk^2}(k_T) = \frac{6A^2}{\frac{A^2}{D_u D_v} D_v} + 2D_u \tag{6.26}$$

$$= 8D_u > 0 \tag{6.27}$$

Which proves that k_T indeed is at a minimum of $B(k)$. Thus k_T is now substituted into equation 6.20 to find B_T:

$$B = 1 + \frac{A^2}{\frac{A^2}{D_u D_v}^{\frac{1}{2}} D_v} + \frac{A^2 D_u}{D_v} + \frac{A^2}{D_u D_v}^{\frac{1}{2}} D_u \tag{6.28}$$

$$= 1 + \frac{A\sqrt{D_u D_v}}{D_v} + \frac{A^2 D_u}{D_v} + \frac{A D_u}{\sqrt{D_u D_v}} \tag{6.29}$$

$$= 1 + \frac{2AD_u D_v}{D_v \sqrt{D_u D_v}} + \frac{A^2 D_u \sqrt{D_u D_v}}{Dv\sqrt{D_u D_v}} \tag{6.30}$$

$$= 1 + 2A\sqrt{\frac{D_u^2}{D_u D_v}} + A^2 \frac{D_u}{D_v} \tag{6.31}$$

$$\Leftrightarrow B_T = (1 + A\eta)^2. \tag{6.32}$$

With $\eta = \sqrt{\frac{D_u}{D_v}}$ the critical value for B_T has been found.

6.4 Alan vs Eberhard

In this section the possibility of a Hopf-bifurcation occuring before Turing instability will be explored. Neglecting the diffusion terms trace and determinant are given by:

$$\tau_{ode} = B - 1 - A^2 \tag{6.33}$$

$$\triangle_{ode} = A^2 \tag{6.34}$$

A Hopf bifurcation happens when imaginary eigenvalues $\lambda_\pm = \frac{1}{2}(\tau \pm \sqrt{\tau^2 - 4\triangle})$ cross the real axis. Which happens when $\tau = 0$, if the determinant if positive. Thus at

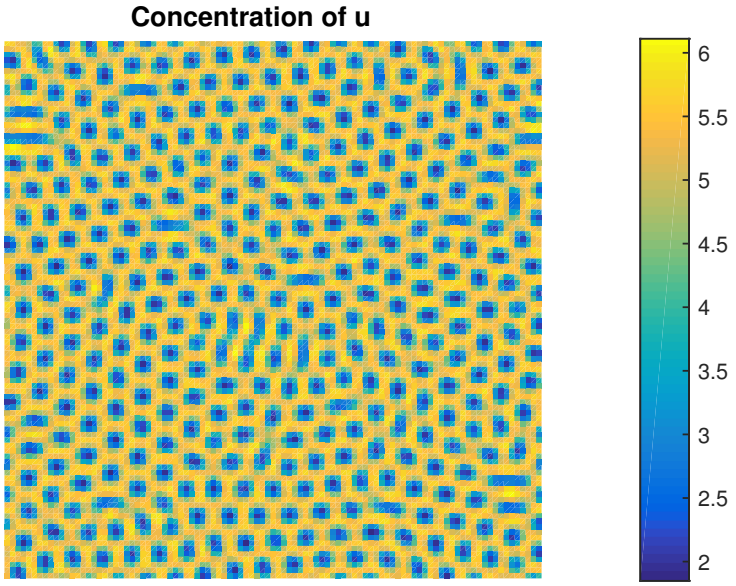

Figure 6.1: Brusselator simulation output for $a = 4.5, b = 7, D_u = 1, D_v = 8$.

$B_H = (1+A^2)$ the system exhibits a Hopf bifurcation as $\triangle_{ode}$ is positive. However Turing instability will occur first if:

$$B_t < B_h \Leftrightarrow (1 + A\eta)^2 < (1 + A^2) \Leftrightarrow 1 + A\eta < \sqrt{1 + A^2} \Leftrightarrow \eta < \frac{\sqrt{1 + A^2} - 1}{A}. \quad (6.35)$$

6.5 Numerical simulations

If B is chosen such that $B > B_T = 6.7132$ if $A = 4.5, D_u = 1$ and $D_v = 8$, various patterns emerge as shown in figure 6.1 . A simulation with `200` instead of `100` grid points for the same input parameters is shown in figure 6.2. If B is increased further it is observed that the concentration of u drops on average, which manifests in expanding blue dots, which show low concentration. At one point the dots merge and form blue lines, which can be seen in figure 6.3.

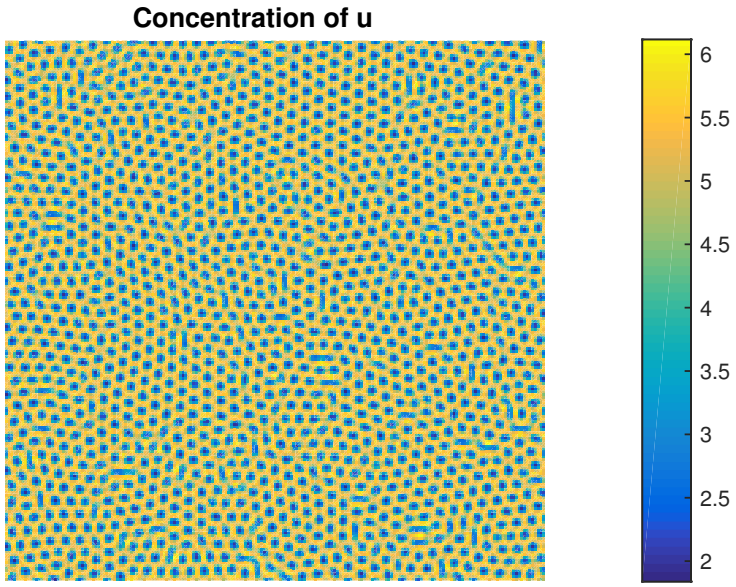

Figure 6.2: Brusselator simulation output for $a = 4.5, b = 7, D_u = 1, D_v = 8$. With twice as many grid points.

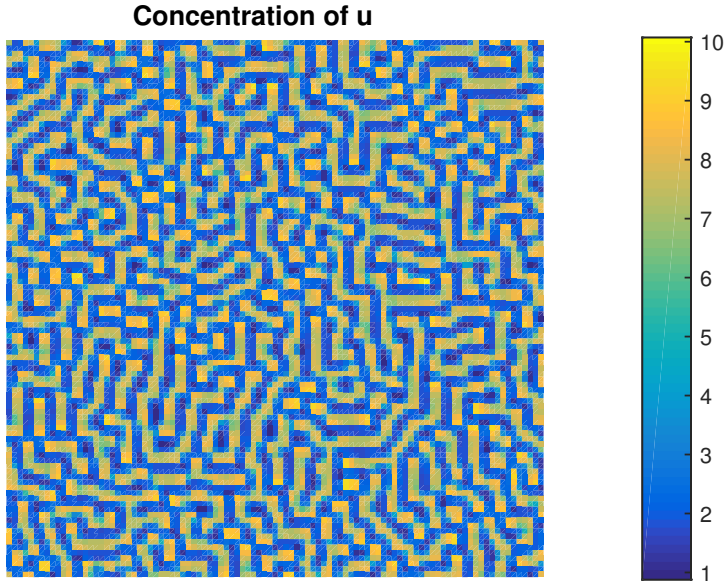

Figure 6.3: Brusselator simulation output for $a = 4.5, b = 9, D_u = 1, D_v = 8$.